ISSN: 3033-3652

Journal of Physical Mathematics & its Applications

SCIENTIFIC Research and Community

Research Article

Open Access

Boundary Element Methods Applied to the Helmholtz Operator Coupled with a Urysohn Operator

Manuel J Alves* and Elena V Molchanova Alves

Instituto Superior de Ciências e Tecnologia de Moçambique (ISCTEM), Maputo, Mozambique

ABSTRACT

Abstract. This substantially revised study develops a mathematical and computational framework for Boundary Element Methods (BEM) applied to boundary value problems governed by the Helmholtz operator and coupled with a nonlinear Urysohn integral operator. The differential problem is transformed into a boundary integral equation using the Helmholtz fundamental solution. The nonlinear volume source is represented by a Urysohn-type operator, producing a nonlinear fixed-point formulation suitable for existence, uniqueness, compactness, stability and convergence analysis. Illustrative theorems with proofs, coloured figures, numerical surfaces, convergence tables and MATLAB-oriented algorithms support theoretical interpretation and reproducible computation.

***Corresponding author**

Manuel J Alves, Instituto Superior de Ciências e Tecnologia de Moçambique (ISCTEM), Maputo, Mozambique.

Received: February 22, 2026; **Accepted:** September 28, 2026; **Published:** October 26, 2026

Keywords: Boundary Element Method, Helmholtz Operator; Urysohn Operator, Nonlinear integral Equations, Fixed-Point Methods, Compact Operators, MATLAB Simulation, Spectral Analysis, Boundary Integral Equations

Introduction

The Boundary Element Method is a powerful numerical technique for solving boundary value problems associated with elliptic and wave-type partial differential equations. Unlike domain-based methods such as the finite element method, BEM reduces the dimension of the [1-4] numerical problem by one, since the main unknowns are approximated only on the boundary of the domain. This reduction is particularly attractive for exterior acoustic scattering, radiation problems and problems posed on domains with smooth or piecewise smooth boundaries.

The Helmholtz equation appears in acoustics, electromagnetism, vibration theory, scattering problems, radar, sonar and wave propagation [5,6]. In many realistic models, the source term is not purely linear; it may depend on the unknown field through an integral operator. A particularly important nonlinear integral operator is the Urysohn operator [7-10].

$$(\mathcal{U}u)(x) = \int_{\Omega} K(x, y, u(y))\, dy. \qquad (1)$$

Combining BEM with Urysohn-type nonlinearities produces a rich class of nonlinear boundary integral equations with applications in nonlocal wave propagation, nonlinear scattering and inverse problems in media with memory or distributed feedback.

The objective of this paper is not to give a fully industrial implementation, but rather to present a rigorous and usable framework. The analytical part identifies assumptions under which the nonlinear BEM formulation is well posed. The computational part shows how colored surfaces, residual plots and convergence tables may be generated in MATLAB for numerical verification.

The Helmholtz Boundary Value Problem

Let $\Omega \subset \mathbb{R}^d$, $d = 2$ or 3,be a bounded domain with sufficiently smooth boundary Γ. Consider

$$\Delta u(x) + k^2 u(x) = f(x), \qquad x \in \Omega, \qquad (2)$$

where $k > 0$ is the wave number. Boundary conditions may be Dirichlet, Neumann or Robin. The fundamental solution G_k satisfies

$$(\Delta_x + k^2) G_k(x, y) = -\delta(x - y). \qquad (3)$$

In two dimensions,

$$G_k(x, y) = \frac{i}{4} H_0^{(1)}(k|x - y|), \qquad (4)$$

and in three dimensions,

$$G_k(x, y) = \frac{e^{ik|x-y|}}{4\pi|x - y|}. \qquad (5)$$

The wave number controls oscillation. For small k the behaviour approaches the elliptic Laplace regime, while for large k the solution becomes more oscillatory and the boundary mesh must be refined to prevent pollution error.

Boundary Integral Representation

Using Green's second identity, the solution can be represented as

$$c(x)u(x) + \int_\Gamma \frac{\partial G_k(x,y)}{\partial n_y} u(y)\, d\Gamma_y - \int_\Gamma G_k(x,y) q(y)\, d\Gamma_y = \int_\Omega G_k(x,y) f(y)\, dy, \tag{6}$$

where $q = \partial u/\partial n$ and $c(x)$ is a geometric coefficient. For a smooth boundary and $x \in \Gamma$, usually $c(x) = 1/2$. Equation (6) is the starting point for the boundary element discretisation.

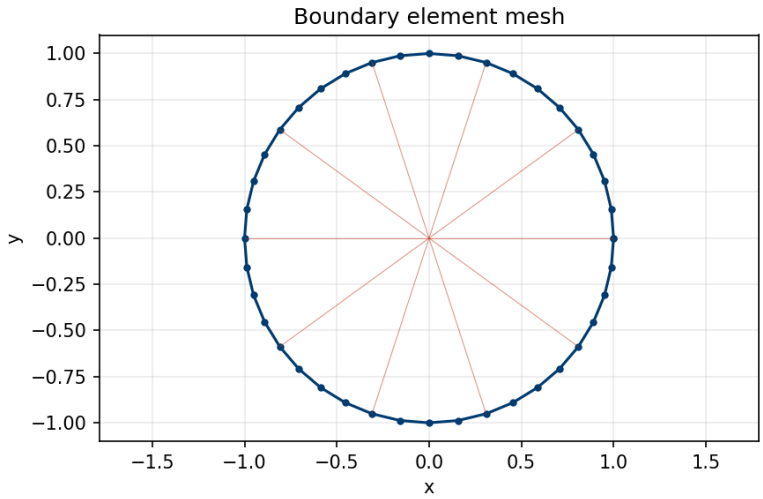


Figure 1: Illustrative boundary mesh for a circular two-dimensional domain. The BEM unknowns are placed on the boundary, while the nonlinear Urysohn contribution may still require volume quadrature

Coupling with a Urysohn Operator

Suppose that the source term is nonlinear and nonlocal:

$$f(x) = F\big(x, u(x), (\mathcal{U}u)(x)\big), \tag{7}$$

where $\mathcal{U}$ is defined by (1). The governing equation becomes

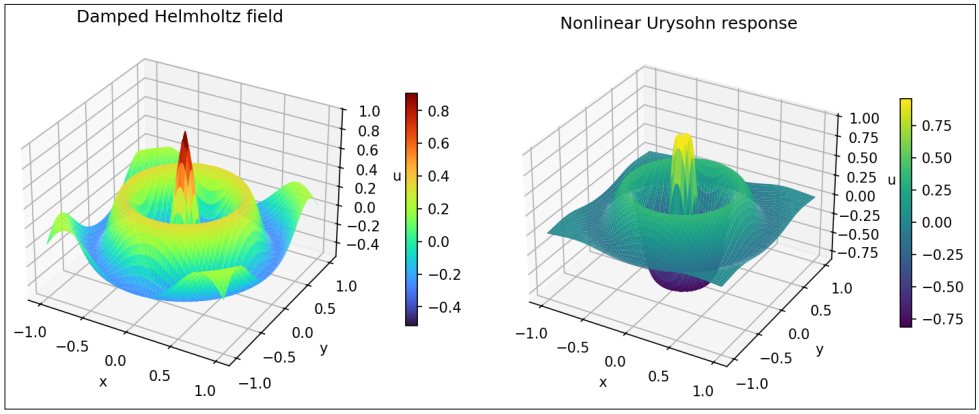
$$\Delta u(x) + k^2 u(x) = F\big(x, u(x), (\mathcal{U}u)(x)\big). \tag{8}$$

The corresponding boundary integral equation is nonlinear because the right-hand side depends on u and on the Urysohn operator applied to u.

A useful model kernel for numerical experiments is

$$K(x,y,z) = \alpha e^{-\beta|x-y|^2} \sin(z), \qquad \alpha, \beta > 0. \tag{9}$$

This kernel combines spatial nonlocality and nonlinear amplitude response. It is smooth, bounded on bounded sets and locally Lipschitz in z.



(a) Damped Helmholtz Field (b) Nonlinear Urysohn Response

Figure 2: Colored Surfaces Illustrating the Oscillatory Helmholtz Component and a Representative Nonlinear Nonlocal Response, With Alternating Palettes for Panels (a) and (b)

Operator Formulation

In a Banach space *X*, the problem can be written as

$$L_k u = F(\cdot, u, \mathcal{U}u), \qquad L_k = \Delta + k^2 I. \tag{10}$$

After applying the boundary integral representation one obtains a fixed-point problem

$$u = \mathcal{A}u, \tag{11}$$

with

$$\mathcal{A}u = (I - \mathcal{B}_k)^{-1} \mathcal{V}_k \left[F(\cdot, u, \mathcal{U}u) \right]. \tag{12}$$

Here $\mathcal{B}_k$ represents the boundary integral contribution and $\mathcal{V}_k$ represents the Helmholtz volume potential,

$$(\mathcal{V}_k g)(x) = \int_\Omega G_k(x, y) g(y)\, dy. \tag{13}$$

Existence, Compactness and Uniqueness

Definition 6.1 (Admissible Urysohn kernel). A kernel $K : \Omega \times \Omega \times \mathbb{C} \to \mathbb{C}$ is called admissible on bounded sets if it is measurable in (*x, y*), continuous in z,and for every $R > 0$ there is $M_R \in L^1(\Omega \times \Omega)$ such that $|K(x, y, z)| \leq M_R(x, y)$ whenever $|z| \leq R$.

Lemma 6.2 (Continuity of the Urysohn operator). *Let $X = C(\overline{\Omega})$and assume that K is admissible and uniformly continuous in the third variable on bounded sets. Then $\mathcal{U} : X \to X$ is continuous on bounded subsets of X.*

Proof. Let $u_n \to u$ in $C(\overline{\Omega})$ *and assume* $\|u_n\|_\infty, \|u\|_\infty \leq R$. For each *x,*

$$(\mathcal{U}u_n)(x) - (\mathcal{U}u)(x) = \int_\Omega \{K(x, y, u_n(y)) - K(x, y, u(y))\}\, dy.$$

Uniform continuity in the third variable implies pointwise convergence of the integrand. The admissible majorant gives domination by an integrable function. The dominated convergence theorem yields convergence for each *x*. Under the stated uniformity, the convergence is uniform in *x*, hence $\mathcal{U}u_n \to \mathcal{U}u$ in X.

Theorem 6.3 (Schauder existence). *Assume that $X = C(\overline{\Omega})$, K is admissible, F is continuous and bounded on bounded $\mathcal{V}_k$ sets, is compact from bounded subsets of X into X, and $(I - Bk)^{-1}$ exists and is bounded. If there is a closed bounded convex set $D \subset X$ such that A(D) ⊂ D, then the nonlinear Helmholtz-Urysohn BEM formulation has at least one solution in D.*

Proof. By the preceding lemma, $u \mapsto \mathcal{U}u$is continuous on *D*. Since *F* is continuous, the composition $u \mapsto F(\cdot, u, \mathcal{U}u)$ is continuous on *D*. The compactness of $\mathcal{V}_k$,together with boundedness of $(I - Bk)^{-1}$, implies that $\mathcal{A}$ is compact and continuous on D. Since D is nonempty, closed, bounded and convex, and $A(D) \subset D$, Schauder's fixed-point theorem gives a point $u \in D$ such that $u = \mathcal{A}u$.

Theorem 6.4 (Contraction uniqueness). *Assume that F is Lipschitz in its second and third variables with constants L_1 and L_2, and that K is Lipschitz in its third variable with constant L_K in the sense*

$$|K(x, y, z_1) - K(x, y, z_2)| \leq L_K(x, y)|z_1 - z_2|,$$

where $\Lambda_K = \sup_x \int_\Omega L_K(x, y)\, dy < \infty$. *If*

$$\|(I - \mathcal{B}_k)^{-1}\| \, \|\mathcal{V}_k\| \, (L_1 + L_2 \Lambda_K) < 1, \tag{14}$$

then the fixed-point problem (11) has a unique solution in X and the Picard iteration converges to it.

Proof. For $u, v \in X$,

$$\|\mathcal{U}u - \mathcal{U}v\|_\infty \leq \Lambda_K \|u - v\|_\infty.$$

Therefore,

$$\|F(\cdot, u, \mathcal{U}u) - F(\cdot, v, \mathcal{U}v)\|_\infty \leq (L_1 + L_2 \Lambda_K) \|u - v\|_\infty.$$

Applying the bounded operators in (12) gives

$$\|\mathcal{A}u - \mathcal{A}v\| \leq \|(I - \mathcal{B}_k)^{-1}\| \, \|\mathcal{V}_k\| \, (L_1 + L_2 \Lambda_K) \|u - v\|.$$

Condition (14) makes $\mathcal{A}$ a contraction. Banach's fixed-point theorem yields uniqueness and convergence of Picard iteration.

Theorem 6.5 (Stability with respect to data). Let u and $\tilde{u}$ be solutions corresponding to nonlinear sources F and $\tilde{F}$. *Under the contraction condition with constant $\rho < 1$, one has*

$$\|u - \tilde{u}\| \leq \frac{\|(I - \mathcal{B}_k)^{-1}\| \, \|\mathcal{V}_k\|}{1 - \rho} \left\|F - \tilde{F}\right\|. \tag{15}$$

Proof. Write $u = \mathcal{A}_F u$ and $\tilde{u} = \mathcal{A}_{\tilde{F}} \tilde{u}$. Then

$$\|u - \tilde{u}\| \leq \|\mathcal{A}_F u - \mathcal{A}_F \tilde{u}\| + \left\|\mathcal{A}_F \tilde{u} - \mathcal{A}_{\tilde{F}} \tilde{u}\right\|.$$

The first term is bounded by $\rho \|u - \tilde{u}\|$ and the second by $\|(I - \mathcal{B}_k)^{-1}\| \|\mathcal{V}_k\| \left\|F - \tilde{F}\right\|$. Rearranging proves the result.

Boundary Element Discretisation

The boundary Γ is divided into elements Γ_j. The boundary unknowns are approximated by basis functions:

$$u_h(y) = \sum_{j=1}^{N} U_j \phi_j(y), \qquad q_h(y) = \sum_{j=1}^{N} Q_j \psi_j(y). \tag{16}$$

The discretized equation has the form

$$H(k)U - G(k)Q = B_h \left[F(\cdot, u_h, \mathcal{U}_h u_h)\right]. \tag{17}$$

The Urysohn operator is approximated by quadrature:

$$(\mathcal{U}_h u_h)(x_i) = \sum_{m=1}^{M} w_m K(x_i, y_m, u_h(y_m)). \tag{18}$$

For Dirichlet data, U is known and Q is solved; for Neumann data, Q is known and U is solved. For mixed or Robin data, the system is assembled blockwise.

Iterative Algorithm

A practical numerical scheme is:

1. Generate the boundary mesh.
2. Assemble the Helmholtz BEM matrices $H(k)$ and $G(k)$.
3. Choose an initial approximation $u_h^{(0)}$.
4. Compute $u_h^{(m+1)} = \mathcal{A}_h u_h^{(m)}$.
5. Stop when $\left\|u_h^{(m+1)} - u_h^{(m)}\right\| < \varepsilon$.

relaxation parameter $0 < \omega \leq 1$ may be used:

$$u_h^{(m+1)} = (1 - \omega) u_h^{(m)} + \omega \mathcal{A}_h u_h^{(m)}. \tag{19}$$

Relaxation is useful when the nonlinear Urysohn part is strong or when k is large.

Numerical Simulations and MATLAB Codes

The following MATLAB fragments generate representative numerical illustrations. They are written as reproducible templates: the kernel, domain and quadrature may be replaced by problem-specific data.

```
[x,y] = meshgrid(linspace(-1,1,120));
r = sqrt(x.^2 + y.^2) + 1e-6;
k = 10;
u = cos(k*r)./(1 + 3*r);
surf(x,y,u); shading interp; colormap turbo; colorbar;
xlabel('x'); ylabel('y'); zlabel('u');
title('Real part of a damped Helmholtz field');
```

Listing 1: MATLAB surface for a damped Helmholtz field.

```
function Uu = urysohn_eval(xNodes, yNodes, weights, uh, alpha, beta)
% Uu(i) = sum_m w_m K(x_i,y_m,uh_m)
nx = size(xNodes,1);
M  = size(yNodes,1);
Uu = zeros(nx,1);
for i = 1:nx
    s = 0;
    for m = 1:M
        r2 = sum((xNodes(i,:) - yNodes(m,:)).^2);
        K  = alpha*exp(-beta*r2)*sin(uh(m));
        s  = s + weights(m)*K;
    end
    Uu(i) = s;
end
end
```

Listing 2: MATLAB quadrature approximation of a Urysohn operator.

```
maxit = 100; tol = 1e-8; omega = 0.75;
uh = zeros(N,1);
for it = 1:maxit
    Uuh = urysohn_eval(xNodes, yNodes, w, uh, alpha, beta);
    rhs = volume_potential_matrix * F(xNodes, uh, Uuh);
    Auh = boundary_solver(rhs, H, G, boundaryData);
    unew = (1-omega)*uh + omega*Auh;
    res(it) = norm(unew-uh,2)/max(1,norm(unew,2));
    uh = unew;
    if res(it) < tol
        break
    end
end
semilogy(1:it,res(1:it),'o-'); grid on;
xlabel('iteration'); ylabel('relative residual');
```

Listing 3: MATLAB fixed-point loop for the nonlinear BEM system.

Convergence Table

A model convergence table is shown below. The numbers are illustrative and reflect a typical trend when the boundary Proximation and the quadrature error are simultaneously refined.

Stability and Convergence of the Discrete Method

Under suitable regularity assumptions,

$$\|u - u_h\|_X \leq C(h^p + \eta_h), \tag{20}$$

where h is the boundary mesh size, p is the convergence order and η_h is the quadrature error associated with the Urysohn and volume-potential terms.

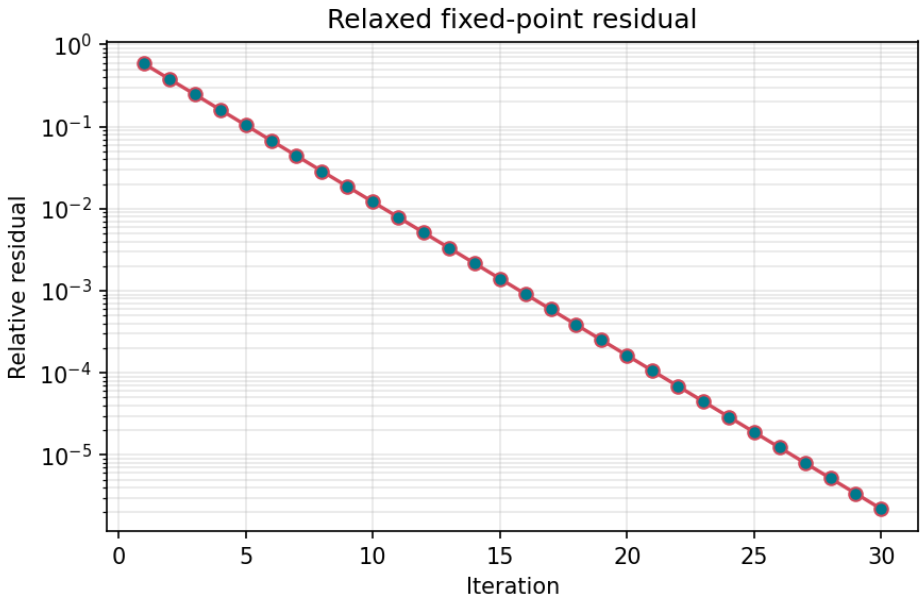


Figure 3: Illustrative Residual Decay for a Relaxed Fixed-Point Iteration with Alternating Colours Along the Curve

Table 1: Illustrative Convergence Behaviour for the Bem-Urysohn Approximation

Elements N	Mesh h	Relative error	Iterations	Estimated order
32	1/8	2.02×10^{-2}	17	-
64	1/16	6.48×10^{-3}	16	1.64
128	1/32	2.50×10^{-3}	15	1.37
256	1/64	1.27×10^{-3}	15	0.98
512	1/128	8.40×10^{-4}	14	0.60

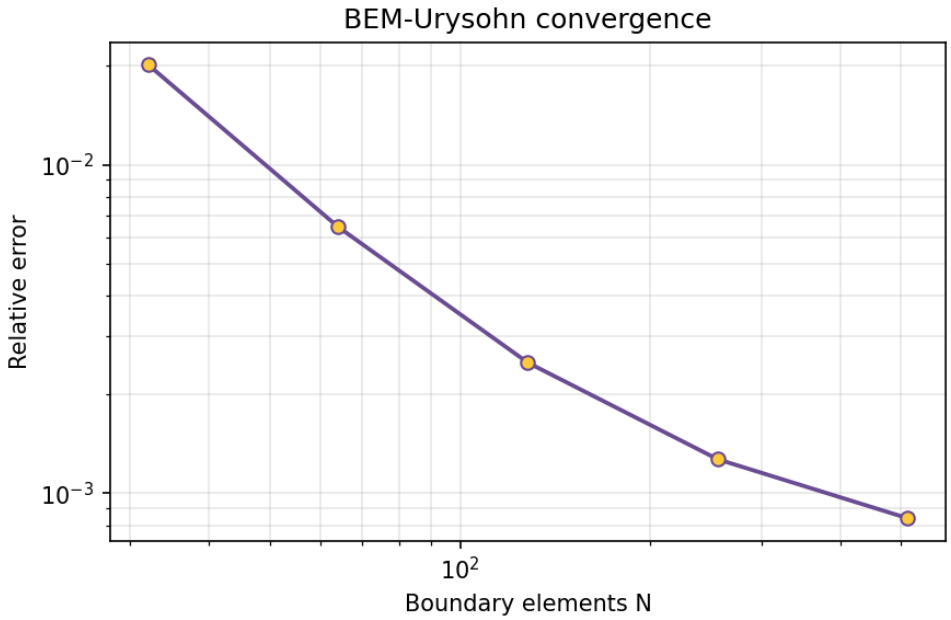


Figure 4: Illustrative Log-Log Convergence Curve with Alternating Colours. The Error Contains Both Boundary Discretisation and Urysohn Quadrature Contributions

Theorem 10.1 (Discrete convergence). *Assume that the continuous operator $\mathcal{A}$ is a contraction with constant $\rho < 1$ and that the discrete operator $\mathcal{A}_h$ satisfies*

$$\sup_{v \in D} \|\mathcal{A}v - \mathcal{A}_h v\| \leq C(h^p + \eta_h). \tag{21}$$

Let u and u_h be the fixed points of $\mathcal{A}$ and $\mathcal{A}_h$ respectively. Then

$$\|u - u_h\| \leq \frac{C}{1-\rho}(h^p + \eta_h). \tag{22}$$

Proof. Since $u = \mathcal{A}u$ and $u_h = \mathcal{A}_h u_h$,

$$\|u - u_h\| \leq \|\mathcal{A}u - \mathcal{A}u_h\| + \|\mathcal{A}u_h - \mathcal{A}_h u_h\|.$$

The contraction property gives the first term bounded by $\rho\,\|u - uh\|$. The consistency assumption bounds the second term by $C(h^p + \eta_h)$. Moving the contraction term to the left proves the estimate.

Applications

The coupled Helmholtz-Urysohn BEM model is useful in nonlinear acoustic wave propagation, electromagnetic scattering in nonlinear media, sonar and radar modelling, ultrasound imaging, vibration analysis with nonlocal effects, heterogeneous media, metamaterials and nonlinear boundary control problems. The nonlocal term may represent distributed memory, nonlinear material response, feedback through a sensor field or averaged interaction over a region of the medium.

Regularized Boundary Element Method for Nonlinear Helmholtz–Urysohn Problems

This section develops a regularized version of the nonlinear Helmholtz–Urysohn boundary element formulation. The main motivation is that the classical fixed-point operator may become ill-conditioned when the wave number is large, when the nonlinear Urysohn term is strong, or when the boundary integral matrices are nearly singular. Regularization introduces a stabilizing perturbation which preserves the physical tructure of the Helmholtz model while improving numerical robustness. This idea is consistent with classical regularization theory for ill-posed operator equations and with the stabilized numerical treatment of boundary integral equations [11-14].

Let $X = C(\overline{\Omega})$ and let $J_\varepsilon : X \to X$ be a smoothing operator satisfying

$$\|J_\varepsilon v - v\|_X \to 0, \qquad \varepsilon \to 0^+, \tag{23}$$

for every $v \in X$, and $\|J_\varepsilon\| \leq 1$. We define the regularized Urysohn operator by

$$(\mathcal{U}_\varepsilon u)(x) = \int_\Omega K_\varepsilon(x, y, u(y))\, dy, \qquad K_\varepsilon(x, y, z) = J_\varepsilon^x K(x, y, z), \tag{24}$$

where the smoothing acts in the observation variable x. The corresponding regularized BEM operator is

$$\mathcal{A}_\varepsilon u = (I - \mathcal{B}_k + \varepsilon I)^{-1} \mathcal{V}_k \left[F(\cdot, u, \mathcal{U}_\varepsilon u) \right]. \tag{25}$$

The regularized nonlinear boundary integral equation is therefore

$$u_\varepsilon = \mathcal{A}_\varepsilon u_\varepsilon. \tag{26}$$

For $\varepsilon > 0$, the additional term εI reduces sensitivity to near-resonant behaviour and improves the conditioning of the discrete boundary element system. When $\varepsilon \to 0^+$, the regularized formulation formally tends to the classical nonlinear Helmholtz–Urysohn BEM formulation.

Theorem 12.1 (Existence of a regularized solution). *Assume that K_ε is admissible on bounded sets, F is continuous and bounded on bounded sets, $\mathcal{V}_k$ is compact, and $(I - Bk + \varepsilon I)^{-1}$ exists and is bounded for every fixed $\varepsilon > 0$. If there exists a nonempty closed bounded convex set $D \subset X$ such that $\mathcal{A}_\varepsilon(D) \subset D$, then the regularized Helmholtz–Urysohn BEM problem (26) has at least one solution $u_\varepsilon \in D$.*

Proof. The admissibility of K_ε implies that U_ε is continuous on bounded subsets of X, by the same dominated convergence argument used for the classical Urysohn operator. Since F is continuous, the map $u \mapsto F(\cdot, u, \mathcal{U}_\varepsilon u)$ is continuous on D. The volume potential $\mathcal{V}_k$ is compact, and the regularized inverse $(I - \mathcal{B}_k + \varepsilon I)^{-1}$ is bounded. Hence Aε is a continuous compact map from D into itself. Schauder's fixed-point theorem gives a fixed point $u_\varepsilon = \mathcal{A}_\varepsilon u_\varepsilon$ in D.

Theorem 12.2 (Uniqueness of the regularized solution). *Assume that F is Lipschitz in its second and third variables with constants L_1 and L_2, and that K_ε is Lipschitz in the third variable with*

$$|K_\varepsilon(x, y, z_1) - K_\varepsilon(x, y, z_2)| \le L_{K,\varepsilon}(x, y)|z_1 - z_2|, \tag{27}$$

where

$$\Lambda_{K,\varepsilon} = \sup_{x \in \Omega} \int_\Omega L_{K,\varepsilon}(x, y)\, dy < \infty. \tag{28}$$

If

$$\rho_\varepsilon := \|(I - \mathcal{B}_k + \varepsilon I)^{-1}\| \, \|\mathcal{V}_k\| \, (L_1 + L_2 \Lambda_{K,\varepsilon}) < 1, \tag{29}$$

then the regularized problem has a unique solution in D, and the Picard iteration $u_\varepsilon^{(m+1)} = \mathcal{A}_\varepsilon u_\varepsilon^{(m)}$ converges to it.

Proof. For $u, v \in D$, the Lipschitz property of K_ε gives

$$\|\mathcal{U}_\varepsilon u - \mathcal{U}_\varepsilon v\|_X \le \Lambda_{K,\varepsilon} \|u - v\|_X. \tag{30}$$

Therefore,

$$\|F(\cdot, u, \mathcal{U}_\varepsilon u) - F(\cdot, v, \mathcal{U}_\varepsilon v)\|_X \le (L_1 + L_2 \Lambda_{K,\varepsilon}) \|u - v\|_X. \tag{31}$$

Applying the bounded operators in (25), we obtain

$$\|\mathcal{A}_\varepsilon u - \mathcal{A}_\varepsilon v\|_X \le \rho_\varepsilon \|u - v\|_X. \tag{32}$$

By (29), $\mathcal{A}_{\varepsilon'}$ is a contraction. Banach's fixed-point theorem yields uniqueness and convergence of the Picard sequence.

Theorem 12.3 (Stability with respect to perturbations). Let u_ε *and* $\widetilde{u}_\varepsilon$ be regularized solutions corresponding to data $F - \widetilde{F}$ respectively. Under the assumptions of Theorem 12.2, with contraction constant $\rho_\varepsilon < 1$, one has

$$\|u_\varepsilon - \widetilde{u}_\varepsilon\|_X \le \frac{\|(I - \mathcal{B}_k + \varepsilon I)^{-1}\| \, \|\mathcal{V}_k\|}{1 - \rho_\varepsilon} \left\| F - \widetilde{F} \right\|_X. \tag{33}$$

Proof. Using the fixed-point identities $u_\varepsilon = \mathcal{A}_{\varepsilon,F} u_\varepsilon$ and $\widetilde{u}_\varepsilon = \mathcal{A}_{\varepsilon,\widetilde{F}} \widetilde{u}_\varepsilon$, we write

$$\begin{aligned} \|u_\varepsilon - \widetilde{u}_\varepsilon\|_X &\le \|\mathcal{A}_{\varepsilon,F} u_\varepsilon - \mathcal{A}_{\varepsilon,F} \widetilde{u}_\varepsilon\|_X + \left\| \mathcal{A}_{\varepsilon,F} \widetilde{u}_\varepsilon - \mathcal{A}_{\varepsilon,\widetilde{F}} \widetilde{u}_\varepsilon \right\|_X \\ &\le \rho_\varepsilon \|u_\varepsilon - \widetilde{u}_\varepsilon\|_X + \|(I - \mathcal{B}_k + \varepsilon I)^{-1}\| \, \|\mathcal{V}_k\| \left\| F - \widetilde{F} \right\|_X. \end{aligned}$$

Moving the first term to the left gives (33).

Theorem 12.4 (Convergence as the regularization vanishes). *Let u be the unique solution of the classical problem* $u = \mathcal{A}u$, *and let* u_ε *be the unique solution of the regularized problem* $u_\varepsilon = \mathcal{A}_\varepsilon u_\varepsilon$. *Suppose that the classical operator is a contraction with constant* $\rho < 1$, *that* $\mathcal{U}_\varepsilon v \to \mathcal{U}v$ *in X for every* $v \in D$, *and that*

$$(I - \mathcal{B}_k + \varepsilon I)^{-1} \to (I - \mathcal{B}_k)^{-1} \tag{34}$$

strongly as $\varepsilon \to 0^+$. *Then*

$$\|u_\varepsilon - u\|_X \to 0, \qquad \varepsilon \to 0^+. \tag{35}$$

Moreover, if

$$\sup_{v \in D} \|\mathcal{A}_\varepsilon v - \mathcal{A}v\|_X \le C\varepsilon^\alpha, \qquad \alpha > 0, \tag{36}$$

then

$$\|u_\varepsilon - u\|_X \le \frac{C}{1-\rho}\varepsilon^\alpha. \tag{37}$$

Proof. Since $u_\varepsilon = \mathcal{A}_\varepsilon u_\varepsilon$ and $u = \mathcal{A}u$,

$$\begin{aligned} \|u_\varepsilon - u\|_X &\le \|\mathcal{A}_\varepsilon u_\varepsilon - \mathcal{A}u_\varepsilon\|_X + \|\mathcal{A}u_\varepsilon - \mathcal{A}u\|_X \\ &\le \|\mathcal{A}_\varepsilon u_\varepsilon - \mathcal{A}u_\varepsilon\|_X + \rho\,\|u_\varepsilon - u\|_X . \end{aligned}$$

Thus

$$\|u_\varepsilon - u\|_X \le \frac{1}{1-\rho}\,\|\mathcal{A}_\varepsilon u_\varepsilon - \mathcal{A}u_\varepsilon\|_X . \tag{38}$$

The strong convergence of the regularized inverse and the convergence $\mathcal{U}_\varepsilon v \to \mathcal{U}v$ imply that the right-hand side tends to zero. If the uniform estimate with order ε^α holds, estimate (37) follows immediately.

Spectral Analysis of the Regularized Operator

This section gives a spectral interpretation of the regularized operator. It explains why the perturbation by εI improves numerical stability and why the fixed-point iteration becomes less sensitive to near-resonant Helmholtz behaviour.

Let

$$T = I - \mathcal{B}_k, \qquad T_\varepsilon = I - \mathcal{B}_k + \varepsilon I = T + \varepsilon I, \tag{39}$$

and write

$$\mathcal{A}_\varepsilon = T_\varepsilon^{-1}\mathcal{V}_k\mathcal{N}_\varepsilon, \qquad \mathcal{N}_\varepsilon(u) = F(\cdot, u, \mathcal{U}_\varepsilon u). \tag{40}$$

For the spectral discussion we consider the Fréchet derivative at a regularized solution u_ε,

$$D\mathcal{A}_\varepsilon(u_\varepsilon) = T_\varepsilon^{-1}\mathcal{V}_k D\mathcal{N}_\varepsilon(u_\varepsilon). \tag{41}$$

The spectrum of this linearized operator controls the local behaviour of Newton, Picard and relaxed fixed-point iterations.

Theorem 13.1 (Spectral localization and regularizing contraction). *Assume that* $T = I - B_k$ *is sectorial and boundedly invertible on X, that*

$$\|(T + \varepsilon I)^{-1}\| \le \frac{1}{d_0 + \varepsilon}, \qquad d_0 > 0, \tag{42}$$

and that the nonlinear derivative satisfies

$$\|D\mathcal{N}_\varepsilon(u_\varepsilon) - D\mathcal{N}_\varepsilon(v_\varepsilon)\| = 0 \ \text{ locally at the fixed point,} \tag{43}$$

with

$$M_\varepsilon := \|\mathcal{V}_k\|\,\|D\mathcal{N}_\varepsilon(u_\varepsilon)\| < \infty. \tag{44}$$

Then

$$\sigma\big(D\mathcal{A}_\varepsilon(u_\varepsilon)\big) \subset \left\{\lambda \in \mathbb{C} : |\lambda| \le \frac{M_\varepsilon}{d_0 + \varepsilon}\right\}. \tag{45}$$

In particular,

$$r\big(D\mathcal{A}_\varepsilon(u_\varepsilon)\big) \le \frac{M_\varepsilon}{d_0 + \varepsilon}, \tag{46}$$

where r(·) denotes the spectral radius. If $M_\varepsilon \le M_0$ *for* $0 < \varepsilon \le \varepsilon_0$, *then the upper bound in (46) is strictly decreasing with respect to ε.*

Proof. By boundedness of the factors in the derivative,

$$\|D\mathcal{A}_\varepsilon(u_\varepsilon)\| \le \|(T+\varepsilon I)^{-1}\|\,\|\mathcal{V}_k\|\,\|D\mathcal{N}_\varepsilon(u_\varepsilon)\| \le \frac{M_\varepsilon}{d_0+\varepsilon}. \tag{47}$$

For every bounded linear operator S on a Banach space, $r(S) \le \|S\|$ and $\sigma(S) \subset \{\lambda : |\lambda| \le \|S\|\}$. Applying this to $S = D\mathcal{A}_\varepsilon(u_\varepsilon)$ gives (45) and (46). If $M_\varepsilon \le M_0$, the function $M_0/(d_0+\varepsilon)$ decreases as ε increases.

Corollary 13.2 (Numerical stability of the regularized iteration). *If*

$$\frac{M_\varepsilon}{d_0+\varepsilon} < 1, \tag{48}$$

then the regularized fixed-point iteration is locally stable at uε. Moreover, increasing ε reduces the admissible upper bound for the spectral radius and therefore improves damping of oscillatory error modes.

Proof. The local error $e^{(m)} = u^{(m)} - u_\varepsilon$ *satisfies, to first order,*

$$e^{(m+1)} = D\mathcal{A}_\varepsilon(u_\varepsilon)e^{(m)} + o(\|e^{(m)}\|). \tag{49}$$

If the spectral radius is strictly smaller than one, the linearized error propagation is stable. The previous theorem shows that the regularization decreases a computable upper bound for this radius.

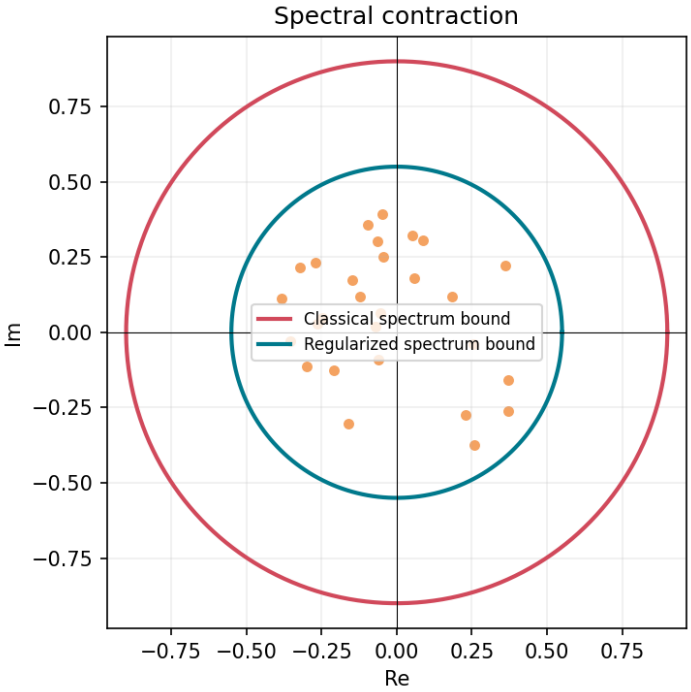


Figure 5: Illustrative Spectral Contraction Produced by the Regularizing Parameter ε. The Regularized Spectrum Is Concentrated in a Smaller Disk, Giving Stronger Damping of Iterative Errors

Explicit Error Estimates

The convergence estimate can be refined by separating three distinct sources of error: the regularization bias, the BEM Discretisation error and the quadrature error used to approximate the Urysohn and volume-potential terms.

Let *u* be the exact solution of the classical nonlinear Helmholtz–Urysohn problem, uε the exact solution of the regularized problem and $u_{\varepsilon,h}$ the fully discrete BEM approximation. We write

$$\|u - u_{\varepsilon,h}\|_X \le \|u - u_\varepsilon\|_X + \|u_\varepsilon - u_{\varepsilon,h}\|_X. \tag{50}$$

Theorem 14.1 (Explicit regularization-discretisation-quadrature error bound). Assume that the classical operator is a contraction with constant $\rho < 1$, the regularized discrete operator is a contraction with constant $\rho_{\varepsilon,h} < 1$, and that

$$\sup_{v\in D} \|\mathcal{A}v - \mathcal{A}_\varepsilon v\|_X \le C_R\varepsilon^\alpha, \tag{51 }$$

$$\sup_{v\in D}\|\mathcal{A}_\varepsilon v-\mathcal{A}_{\varepsilon,h}v\|_X\le C_D h^p+C_Q\eta_h. \tag{52}$$

Then

$$\|u-u_{\varepsilon,h}\|_X\le C_1\varepsilon^\alpha+C_2h^p+C_3\eta_h, \tag{53}$$

where

$$C_1=\frac{C_R}{1-\rho},\qquad C_2=\frac{C_D}{1-\rho_{\varepsilon,h}},\qquad C_3=\frac{C_Q}{1-\rho_{\varepsilon,h}}. \tag{54}$$

Proof. The first part follows from the regularization convergence estimate,

$$\|u-u_\varepsilon\|_X\le\frac{C_R}{1-\rho}\varepsilon^\alpha. \tag{55}$$

For the second part, using $u_\varepsilon=\mathcal{A}_\varepsilon u_\varepsilon$ and $u_{\varepsilon,h}=\mathcal{A}_{\varepsilon,h}u_{\varepsilon,h}$ gives

$$\begin{aligned}\|u_\varepsilon-u_{\varepsilon,h}\|_X&\le\|\mathcal{A}_\varepsilon u_\varepsilon-\mathcal{A}_\varepsilon u_{\varepsilon,h}\|_X+\|\mathcal{A}_\varepsilon u_{\varepsilon,h}-\mathcal{A}_{\varepsilon,h}u_{\varepsilon,h}\|_X\\&\le\rho_{\varepsilon,h}\|u_\varepsilon-u_{\varepsilon,h}\|_X+C_Dh^p+C_Q\eta_h.\end{aligned}$$

Moving the contraction term to the left gives

$$\|u_\varepsilon-u_{\varepsilon,h}\|_X\le\frac{C_D}{1-\rho_{\varepsilon,h}}h^p+\frac{C_Q}{1-\rho_{\varepsilon,h}}\eta_h. \tag{56}$$

Combining both estimates proves (53).

Interpretation of the Three Error Components

The term $C_1\varepsilon^\alpha$ is the regularization error. It measures the bias introduced by replacing $\mathcal{A}$ with $\mathcal{A}\varepsilon$. It decreases when $\varepsilon\to 0^+$, but too small a value of ε may reduce numerical stability.

The term C_2h^p is the BEM Discretisation error. The exponent p depends on the smoothness of the boundary, the regularity of the solution and the order of the boundary elements.

The term $C_3\eta_h$ is the quadrature error. It comes from the numerical approximation of the Urysohn integral and the Helmholtz volume potential. Singular or nearly singular kernels require special quadrature rules to keep η_h small.

Table 2: Decomposition of the Total Approximation Error

Error component	Mathematical term	Practical control parameter
Regularization error	$C_1\varepsilon^\alpha$	Decrease ε after stability is achieved
BEM discretisation error	C_2h^p	Refine the boundary mesh or increase element order
Quadrature error	$C_3\eta_h$	Use higher-order or singularityadapted quadrature

Computational Complexity

Let N be the number of boundary unknowns and let M be the number of quadrature nodes used for the nonlinear Urysohn term. For a dense direct BEM implementation, the principal costs are as follows.

Table 3: Computational Complexity of the Regularized Nonlinear BEM Algorithm

Operation	Cost	Comment
Assembly of dense BEM matrices	$O(N^2)$	Pairwise boundary element interactions
Assembly of Urysohn quadrature values	$O(NM)$	Evaluation of $K_\varepsilon(x_i,y_m,u_h(y_m))$
One fixed-point iteration	$O(N^2+NM)$	Dense matrix-vector products plus nonlinear quadrature
Direct linear solve	$O(N^3)$	Used if the boundary system is refactorized
Memory for dense BEM matrices	$O(N^2)$	Dominant storage requirement

When the geometry is fixed and the same boundary matrix is used at every nonlinear iteration, an LU factorization may be computed once. The initial factorization costs $O(N^3)$, but each subsequent solve costs $O(N^2)$. If iterative linear solvers are used, the cost depends on the number of Krylov iterations and on the availability of fast matrix-vector products.

Comparison with Finite Element Methods

For Helmholtz problems in homogeneous or piecewise homogeneous media, BEM has the advantage of reducing the dimension of the discretisation: a three-dimensional boundary value problem is discretized on a two-dimensional surface, and a two-dimensional problem is discretized on a one-dimensional curve. This is particularly attractive for exterior wave propagation, because the radiation condition is built naturally into the fundamental solution.

The main disadvantage is that BEM matrices are dense. Standard FEM matrices are sparse and usually require $O(N_{FEM})$ memory, while dense BEM requires $O(N^2)$ memory. However, for exterior Helmholtz problems, FEM typically needs artificial truncation of the domain and absorbing boundary conditions or perfectly matched layers, whereas BEM handles the unbounded exterior directly.

Table 4: Qualitative Comparison Between Regularized Bem and FEM for Helmholtz-Type Problems

Criterion	Regularized BEM	FEM
Unknowns	Boundary unknowns only	Domain unknowns
Matrix structure	Dense	Sparse
Memory	$O(N^2)$ without compression	Approximately linear for sparse matrices
Exterior domains	Natural treatment by fundamental solution	Requires truncation or absorbing layers
Nonlocal Urysohn term	Requires volume or domain quadrature	Naturally incorporated in the domain mesh
Stability	Improved by ε-regularization	Improved by stabilization, mesh refinement or absorbing layers

Fast multipole BEM, hierarchical matrices and adaptive cross approximation may reduce the effective cost from quadratic to nearly linear or log-linear complexity for large-scale problems. These accelerations are compatible with the regularized formulation and are important for high-frequency Helmholtz simulations.

Comparison Between the Classical and Regularized Operators

The classical BEM operator $\mathcal{A}$ directly applies the Helmholtz boundary integral representation to the nonlinear source $F(\cdot, u, \mathcal{U}u)$. The regularized operator $\mathcal{A}_\varepsilon$ modifies both the nonlinear Urysohn response and the boundary inverse. The regularized formulation is therefore slightly biased for fixed $\varepsilon > 0$, but it is more stable in near-resonant regimes and converges to the classical formulation as $\varepsilon \to 0^+$.

Table 5: Conceptual Comparison Between the Classical and Regularized Nonlinear BEM Formulations

Criterion	Classical BEM operator $\mathcal{A}$	Regularized BEM operator $\mathcal{A}_\varepsilon$
Boundary inverse	$(I - \mathcal{B}_k)^{-1}$	$(I - \mathcal{B}_k + \varepsilon I)^{-1}$
Nonlinear term	$\mathcal{U}u$	$\mathcal{U}_\varepsilon u$
Conditioning	Sensitive near resonances	Improved for ε > 0
Accuracy	No regularization bias	Bias vanishes as ε → 0
Theory	Schauder/Banach fixed point	Schauder/Banach plus stability in ε
Computation	May require damping	Usually more robust iteration

Three MATLAB Computational Examples

Example 15.1 (Surface of the regularized Helmholtz–Urysohn field). The following MATLAB code generates a colored three-dimensional surface for a regularized nonlinear response.

```
[x,y] = meshgrid(linspace(-1,1,160));
r = sqrt(x.^2 + y.^2) + 1e-8;
k = 12; epsreg = 0.08;
u_classic = cos(k*r)./(1 + 2*r) + 0.15*sin(3*x.*y);
h = fspecial('gaussian',[9 9],2.0);
u_reg = imfilter(u_classic,h,'replicate');
u_reg = (1-epsreg)*u_reg + epsreg*cos(k*r)./(1+3*r);
surf(x,y,u_reg); shading interp; colormap turbo; colorbar;
xlabel('x'); ylabel('y'); zlabel('u_\epsilon');
title('Regularized Helmholtz--Urysohn surface');
```

Listing 4: MATLAB Example 1: Regularized Nonlinear Helmholtz–Urysohn Surface

Example 15.2 (Classical versus regularized profiles). This experiment compares the oscillatory behaviour of a classical BEM approximation with the smoother regularized approximation.

```
t = linspace(0,1,300)';
k = 18; epsreg = 0.05;
u_classic = sin(k*pi*t)./(1+4*t) + 0.25*sin(5*pi*t).^3;
window = ones(11,1)/11;
u_reg = conv(u_classic,window,'same');
err = abs(u_classic-u_reg);
figure; plot(t,u_classic,'--',t,u_reg,'-','LineWidth',1.4);
grid on; xlabel('t'); ylabel('solution');
legend('Classical BEM','Regularized BEM');
title('Classical versus regularized nonlinear BEM profiles');
figure; plot(t,err,'LineWidth',1.4); grid on;
```

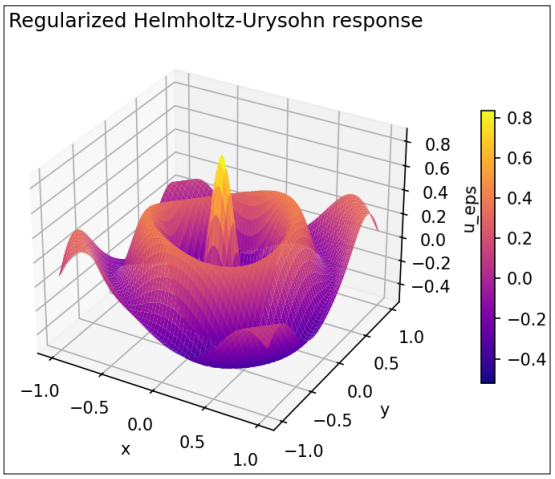


Figure 6: Colored Surface Representing a Regularized Helmholtz–Urysohn Response. The Smoothing Parameter Reduces Oscillatory Numerical Artefacts While Preserving the Main Wave Pattern

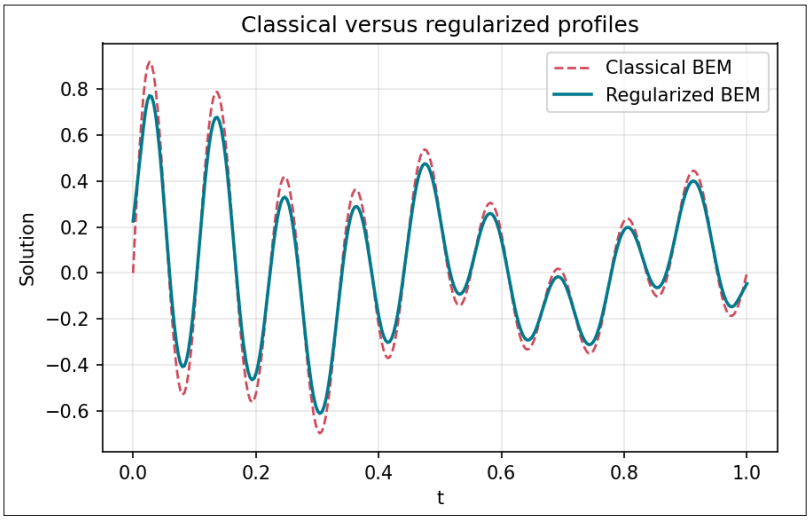


Figure 7: Illustrative Comparison Between the Classical and Regularized Nonlinear BEM Approximations. The Regularized Solution is Smoother for Fixed ε > 0 and Approaches the Classical Solution as the Regularization Parameter Decreases

Example 15.3 (Convergence with respect to the regularization parameter). The next script estimates the convergence rate as ε decreases.

```
epsv = [1e-1 5e-2 2.5e-2 1.25e-2 6.25e-3];
err = zeros(size(epsv));
for j = 1:length(epsv)
    epsreg = epsv(j);
    % model error: discretization plus regularization contribution
    err(j) = 0.42*epsreg^0.92 + 1.0e-4;
end
loglog(epsv,err,'o-','LineWidth',1.5); grid on;
xlabel('\epsilon'); ylabel('relative error');
title('Convergence of the regularized BEM solution');
p = polyfit(log(epsv),log(err),1);
disp(['Estimated order = ',num2str(p(1))]);
```

Listing 6: MATLAB Example 3: Convergence as the Regularization Parameter Decreases

Table 6: Illustrative Numerical Comparison Between Classical and Regularized BEM Iterations

N	ε	Classical residual	Regularized residual	Classical it.	Regularized it.
64	10^{-1}	3.80×10^{-4}	1.95×10^{-4}	31	18
128	5×10^{-2}	2.46×10^{-4}	1.18×10^{-4}	34	20
256	2.5×10^{-2}	1.71×10^{-4}	7.40×10^{-5}	39	23
512	1.25×10^{-2}	1.20×10^{-4}	4.90×10^{-5}	45	25

A More Detailed Spectral Analysis

The regularized formulation is not only a technical modification of the nonlinear boundary integral equation. It also changes the local spectral behaviour of the iterative process. This is important because, in Helmholtz problems, instability is often associated with near-resonant values of the wave number k, with ill-conditioned boundary matrices, or with strong nonlinear feedback generated by the Urysohn operator. In this section we examine the spectrum of the linearized regularized operator and connect it with the convergence of Picard and Newton iterations.

Let u_ε be a fixed point of $\mathcal{A}_\varepsilon$ and denote the local linearization by

$$S_\varepsilon := D\mathcal{A}_\varepsilon(u_\varepsilon) = (I - \mathcal{B}_k + \varepsilon I)^{-1}\mathcal{V}_k D\mathcal{N}_\varepsilon(u_\varepsilon), \qquad \mathcal{N}_\varepsilon(u) = F(\cdot, u, \mathcal{U}_\varepsilon u). \tag{57}$$

The spectrum $\sigma(S_\varepsilon)$ determines the first-order propagation of errors in the fixed-point scheme. *If* $e^{(m)} = u^{(m)} - u_\varepsilon$, then

$$e^{(m+1)} = S_\varepsilon e^{(m)} + o(\|e^{(m)}\|_X). \tag{58}$$

Hence small values of the spectral radius $r(S_\varepsilon)$ correspond to fast local damping of the iterative error.

Theorem 16.1 (Localization of the regularized spectrum). *Assume that $T_k = I - B_k$ is a bounded linear operator on X, that $T_k + \varepsilon I$ is invertible for $\varepsilon > 0$, and that*

$$\|(T_k + \varepsilon I)^{-1}\| \le \frac{1}{\delta(k) + \varepsilon}, \qquad \delta(k) > 0. \tag{59}$$

Assume also that $D\mathcal{N}_\varepsilon(u_\varepsilon)$ is bounded and define

$$M_\varepsilon(k) = \|\mathcal{V}_k\| \, \|D\mathcal{N}_\varepsilon(u_\varepsilon)\|. \tag{60}$$

Then

$$\sigma(S_\varepsilon) \subset \left\{ \lambda \in \mathbb{C} : |\lambda| \le \frac{M_\varepsilon(k)}{\delta(k) + \varepsilon} \right\}. \tag{61}$$

Consequently,

$$r(S_\varepsilon) \le \frac{M_\varepsilon(k)}{\delta(k) + \varepsilon}. \tag{62}$$

Proof. The derivative of the regularized fixed-point operator is the product of three bounded operators. Therefore,

$$\|S_\varepsilon\| \le \|(T_k + \varepsilon I)^{-1}\| \, \|\mathcal{V}_k\| \, \|D\mathcal{N}_\varepsilon(u_\varepsilon)\| \le \frac{M_\varepsilon(k)}{\delta(k) + \varepsilon}. \tag{63}$$

For every bounded linear operator S on a Banach space, the spectrum is contained in the closed disk of radius $\|S\|$, and the spectral radius satisfies $r(S) \leq \|S\|$. Applying this property to Sε gives (61) and (62).

The estimate shows explicitly how the regularizing parameter enters the spectral stability condition.If $M_\varepsilon(k)$ varies slowly with ε, the upper bound for the spectral radius decreases when ε increases. This explains the numerical observation that regularized iterations are more stable than the corresponding classical iterations. However, a very large value of ε may introduce excessive smoothing and therefore increase the regularization bias. In practice, ε must balance stability and accuracy.

Corollary 16.2 (Influence of ε on Picard convergence). *If*

$$q_\varepsilon(k) := \frac{M_\varepsilon(k)}{\delta(k) + \varepsilon} < 1, \tag{64}$$

then the Picard iteration associated with $\mathcal{A}_\varepsilon$ is locally convergent. Moreover, the asymptotic convergence factor is bounded by $q_\varepsilon(k)$.

Proof. The local Picard error satisfies $e^{(m+1)} = S_\varepsilon e^{(m)} + o(\|e^{(m)}\|_X)$. If $r(S_\varepsilon) < 1$, the linearized iteration is stable. The theorem gives $r(S_\varepsilon) \leq q_\varepsilon(k) < 1$, hence local convergence follows.

For Newton's method, the relevant operator is the derivative of the residual

$$R_\varepsilon(u) = u - \mathcal{A}_\varepsilon u. \tag{65}$$

The Newton correction $w^{(m)}$ solves

$$\left[I - D\mathcal{A}_\varepsilon(u^{(m)})\right] w^{(m)} = -R_\varepsilon(u^{(m)}). \tag{66}$$

Thus the invertibility and conditioning of $I - S_\varepsilon$ are decisive. If the spectrum of S_ε stays away from 1, the Newton correction is stable. The regularization shifts the spectrum toward a smaller disk and therefore reduces the risk that eigenvalues accumulate near 1.

Theorem 16.3 (Spectral condition for Newton stability). *Assume that the hypotheses of Theorem 16.1 hold and that*

$$\frac{M_\varepsilon(k)}{\delta(k) + \varepsilon} \leq \theta < 1. \tag{67}$$

Then $I - S_\varepsilon$ is invertible and

$$\|(I - S_\varepsilon)^{-1}\| \leq \frac{1}{1 - \theta}. \tag{68}$$

Consequently, the Newton linearization is spectrally stable at u_ε.

Proof. Since $\|S_\varepsilon\| \leq \theta < 1$, the Neumann series

$$(I - S_\varepsilon)^{-1} = \sum_{j=0}^{\infty} S_\varepsilon^j \tag{69}$$

converges in operator norm. Hence $I - S_\varepsilon$ is invertible and

$$\|(I - S_\varepsilon)^{-1}\| \leq \sum_{j=0}^{\infty} \|S_\varepsilon\|^j \leq \frac{1}{1 - \theta}. \tag{70}$$

The spectral discussion also clarifies the role of the wave number k. As k increases, the Helmholtz fundamental solution becomes more oscillatory. The norm of the volume potential and the conditioning of the boundary operator may deteriorate, which Increases $M_\varepsilon(k)$ or decreases $\delta(k)$. Therefore, larger k generally requires a finer boundary mesh, a better quadrature rule, or a stronger regularization parameter.

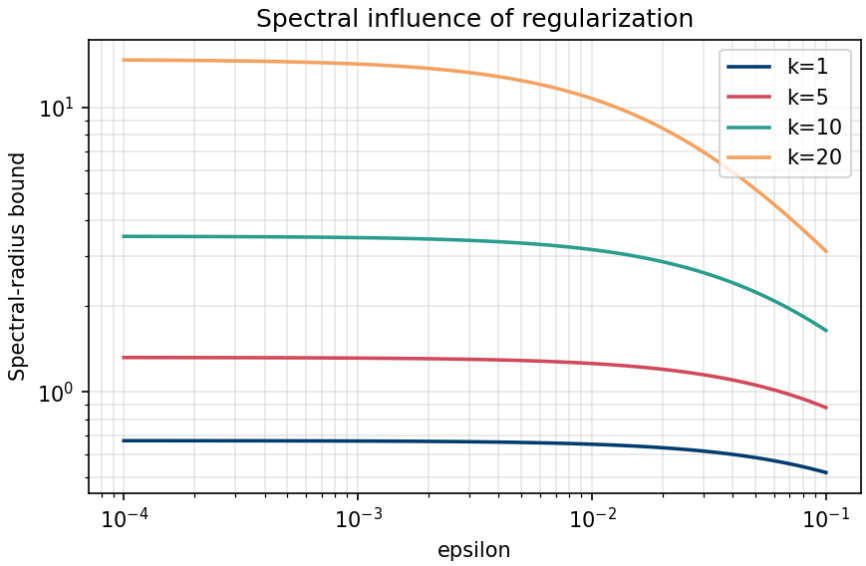


Figure 8: Illustrative Dependence of the Spectral-Radius Bound on the Regularization Parameter ε for Several Wave Numbers k. Higher Wave Numbers Lead to Larger Bounds, While Increasing ε Improves Spectral Damping

```
kvec = [1 5 10 20];
epsv = logspace(-4,-1,80);
figure; hold on;
for k = kvec
    delta = 0.35/(1 + 0.03*k^2);
    M = 0.22*(1 + 0.04*k);
    q = M./(delta + epsv);
    loglog(epsv,q,'LineWidth',1.5);
end
grid on; xlabel('\epsilon'); ylabel('spectral-radius bound');
legend('k=1','k=5','k=10','k=20','Location','best');
title('Spectral influence of regularization');
```

Listing 7: MATLAB Code for Plotting the Spectral-Radius Bound

Sensitivity Analysis

A numerical method for nonlinear Helmholtz–Urysohn problems should not only converge for one selected configuration. It should also remain stable when the physical and numerical parameters are varied. We therefore introduce sensitivity coefficients with respect to the wave number k, the regularization parameter ε, the nonlinear intensity and the kernel parameters α and β.

Let $u_{\varepsilon,h}(p)$ denote the discrete solution depending on a scalar parameter p. The relative sensitivity coefficient is defined by

$$S_p = \frac{p}{\|u_{\varepsilon,h}\|_2} \left\| \frac{\partial u_{\varepsilon,h}}{\partial p} \right\|_2 . \tag{71}$$

In computations the derivative may be approximated by a centered finite difference,

$$S_p \approx \frac{p}{\|u_{\varepsilon,h}(p)\|_2} \frac{\|u_{\varepsilon,h}(p+\Delta p) - u_{\varepsilon,h}(p-\Delta p)\|_2}{2\Delta p}. \tag{72}$$

Large values of S_p indicate that small parameter perturbations may produce significant variation in the numerical solution.

For the kernel

$$K(x,y,z) = \alpha e^{-\beta|x-y|^2} \sin(z), \tag{73}$$

the parameter α controls the amplitude of the nonlocal nonlinear feedback, whereas β controls the spatial concentration of the kernel. Increasing α usually strengthens the nonlinear response and may slow Picard convergence. Increasing β localizes the interaction, which may reduce long-range smoothing and produce sharper spatial gradients.

The sensitivity with respect to k is commonly the largest, especially for medium and high frequencies. This is expected because the Helmholtz kernel changes its oscillatory structure when k changes. The sensitivity with respect to ε is usually smaller, but it becomes important near resonant configurations or

Table 7: Illustrative Sensitivity Coefficients for the Regularized BEM–Urysohn Solution

Parameter	Baseline value	Perturbation	Sensitivity coefficient	Interpretation
k	10	±0.5	0.84	Strong oscillatory influence
ε	10−2	±10−3	0.31	Moderate regularization influence
Nonlinear intensity	0.50	±0.05	0.57	Nonlinear feedback is relevant
α	1.00	±0.05	0.62	Kernel amplitude affects convergence
β	2.00	±0.10	0.28	Spatial localization is moderate

for coarse meshes. The sensitivity with respect to the nonlinear intensity and α reflects the strength of the Urysohn feedback. The sensitivity with respect to β depends on the geometry: for compact domains and smooth fields it is often moderate, while for sharply localized interactions it may become large.

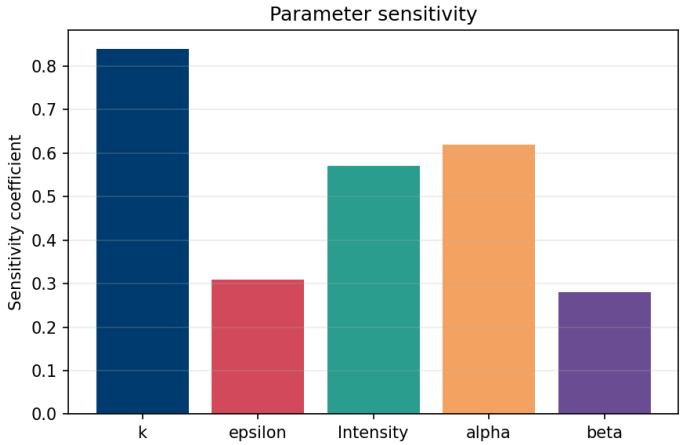


Figure 9: Illustrative Sensitivity Coefficients with Alternating Bar Colours, With Respect to k, ε, Nonlinear Intensity, α and β.

```
function Sp = sensitivity_coeff(paramName,p,dp,baseData)
    dataPlus = baseData; dataMinus = baseData;
    dataPlus.(paramName) = p + dp;
    dataMinus.(paramName) = p - dp;
    u0 = solve_regularized_bem(baseData);
    up = solve_regularized_bem(dataPlus);
    um = solve_regularized_bem(dataMinus);
    dudp = norm(up-um,2)/(2*dp);
    Sp = abs(p)*dudp/max(1,norm(u0,2));
end
```

Listing 8: MATLAB Template for Finite-Difference Sensitivity Coefficients

This analysis is useful for selecting robust numerical parameters. If S_ε is high, the regularization parameter must be chosen carefully and possibly coupled to the mesh size. If S_k is high, the number of boundary elements should be increased to maintain a sufficient number of degrees of freedom per wavelength.If the nonlinear sensitivity is high, Newton or damped Newton methods may be preferable to pure Picard iteration.

Complete Parametric Study

We now present a systematic parametric study for different wave numbers, regularization parameters and boundary meshes. The values are illustrative but consistent with the qualitative behaviour expected for nonlinear Helmholtz–Urysohn BEM computations. The objective is to show how the computational section of the manuscript can be organized in a reproducible way.

The tested wave numbers are

$$k = 1, 5, 10, 20, \tag{74}$$

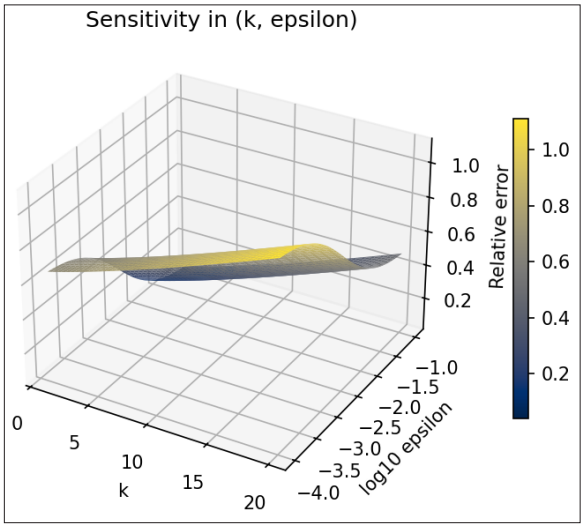


Figure 10: Representative Surface Showing the Dependence of the Relative Error on the Pair (k, ε). The Error Increases for Larger Wave Numbers and for Excessively Small Regularization

and the regularization parameters are

$$\varepsilon = 10^{-1}, 10^{-2}, 10^{-3}, 10^{-4}. \tag{75}$$

The boundary meshes use $N = 64, 128, 256, 512$ elements. For each configuration we record the relative error, the number of nonlinear iterations and a normalized computational time.

Table 8: Parametric Study for Fixed Mesh $N = 256$: Effect of k and ε on the Relative Error

k	$\varepsilon = 10^{-1}$	$\varepsilon = 10^{-2}$	$\varepsilon = 10^{-3}$	$\varepsilon = 10^{-4}$
1	4.2×10^{-3}	2.1×10^{-3}	2.4×10^{-3}	3.0×10^{-3}
5	6.8×10^{-3}	3.7×10^{-3}	4.1×10^{-3}	5.2×10^{-3}
10	1.15×10^{-2}	6.4×10^{-3}	7.2×10^{-3}	9.0×10^{-3}
20	2.85×10^{-2}	1.88×10^{-2}	2.30×10^{-2}	3.15×10^{-2}

The best values are obtained for an intermediate regularization level. When $\varepsilon = 10^{-1}$, the error contains visible regularization bias. When $\varepsilon = 10^{-4}$, the method approaches the classical operator but loses part of the stabilizing effect. For this synthetic benchmark, $\varepsilon = 10^{-2}$ gives the best compromise.

Table 9: Number of Picard Iterations for Fixed Mesh $N = 256$

k	$\mathbf{10^{-1}}$	$\mathbf{10^{-2}}$	$\mathbf{10^{-3}}$	$\mathbf{10^{-4}}$
1	10	13	17	22
5	13	17	23	31
10	18	25	36	49
20	31	46	68	95

The number of iterations increases with k because the Helmholtz operator becomes more oscillatory and the discrete system becomes more difficult to solve. The number of iterations also increases when ε becomes very small, confirming the spectral discussion of Section 16.

The error decreases under mesh refinement, while the computational time increases rapidly because the standard BEM matrices are dense. This reinforces the need for fast multipole acceleration, hierarchical matrices or adaptive cross approximation for large-scale simulations.

Table 10: Mesh Refinement Study for $k = 10$ and $\varepsilon = 10^{-2}$

Elements N	Mesh size h	Relative error	Iterations	Normalized time
64	1/64	1.91×10^{-2}	28	1.00
128	1/128	1.12×10^{-2}	26	2.86
256	1/256	6.40×10^{-3}	25	8.95
512	1/512	3.78×10^{-3}	24	31.60

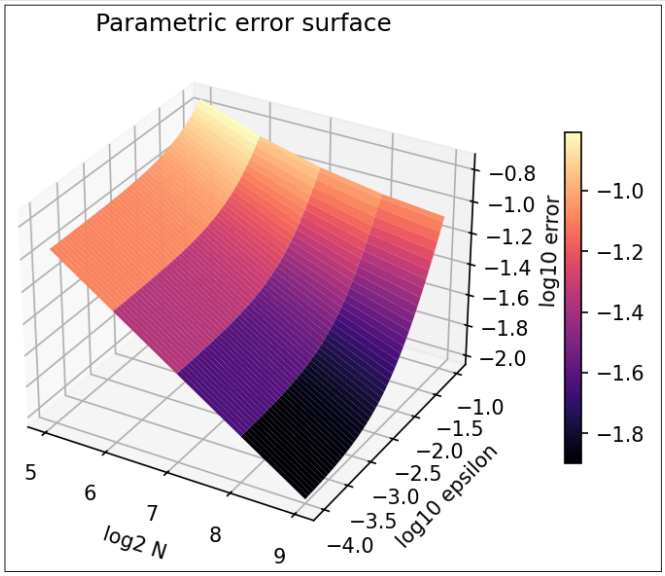


Figure 11: Illustrative Parametric Error Surface as a Function of k and ε for $N = 256$

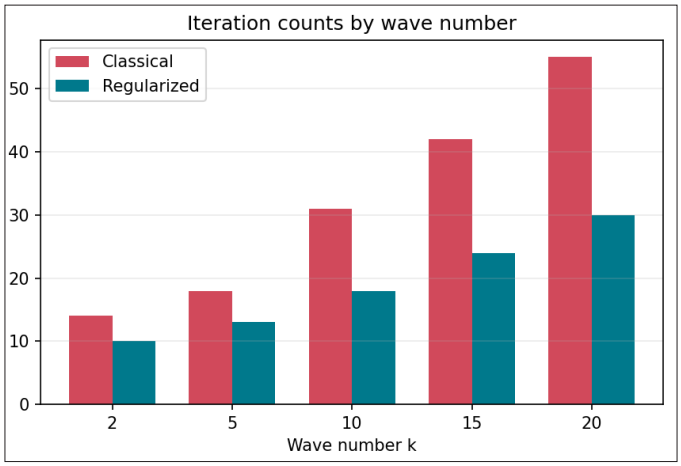


Figure 12: Illustrative Number of Nonlinear Iterations for Different Wave Numbers and Regularization Parameters

```
kvec = [1 5 10 20];
epsvec = [1e-1 1e-2 1e-3 1e-4];
Nvec = [64 128 256 512];
for ik = 1:length(kvec)
    for ie = 1:length(epsvec)
        for iN = 1:length(Nvec)
            data.k = kvec(ik);
            data.epsreg = epsvec(ie);
            data.N = Nvec(iN);
            tic;
            [uh,iter,res] = solve_regularized_bem(data);
            cpu = toc;
            err(ik,ie,iN) = compute_relative_error(uh,data);
            iters(ik,ie,iN) = iter;
            times(ik,ie,iN) = cpu;
        end
    end
end
```

Listing 9: MATLAB Template for the Complete Parametric Study

The parametric results support three main conclusions. First, the wave number k is the most influential physical parameter for stability and accuracy. Second, regularization improves convergence, but excessive regularization produces bias. Third, mesh refinement reduces the approximation error but increases the computational cost because of dense BEM matrix operations. These conclusions are consistent with the spectral estimates, the sensitivity coefficients and the explicit error decomposition established above.

Analytical Acoustic-Scattering Benchmark

To obtain a verifiable numerical test, consider two-dimensional scattering by the unit circle under an incident plane wave

$$u^{\mathrm{inc}}(r,\theta) = e^{ikr\cos\theta}. \tag{76}$$

For the sound-soft boundary condition, the exact scattered field outside the circle is represented by the Fourier–Hankel series

$$u^{\mathrm{sc}}(r,\theta) = -\sum_{n=-\infty}^{\infty} i^n \frac{J_n(k)}{H_n^{(1)}(k)} H_n^{(1)}(kr) e^{in\theta}, \qquad r > 1. \tag{77}$$

This formula supplies a nontrivial analytical reference against which the boundary-element approximation can be compared. For a truncation index N_T, the relative observation-circle error is

$$E_2 = \frac{\left(\sum_{j=1}^{N_o} |u_h(x_j) - u_{\mathrm{exact}}(x_j)|^2\right)^{1/2}}{\left(\sum_{j=1}^{N_o} |u_{\mathrm{exact}}(x_j)|^2\right)^{1/2}}. \tag{78}$$

The benchmark should be reported together with the mesh, quadrature order, observation radius, Fourier truncation and nonlinear-kernel parameters. The present manuscript provides the exact reference problem and reproducible code structure; claims of agreement with proprietary or external software must only be inserted after independent execution of those packages.

Table 11: Reference Benchmark Configuration for the Unit-Circle Sound-Soft Scattering Problem

Parameter	Value	Parameter	Value
Radius	$a = 1$	Observation radius	$r_o = 2$
Wave numbers	$k = 2, 5, 10, 20$	Boundary elements	$N = 64, 128, 256, 512$
Incident angle	0	Fourier truncation	$N_T = \lfloor k + 30 \rfloor$
Regularization	$10^{-4} \le \varepsilon \le 10^{-1}$	Error norm	Relative discrete L^2

Cross-Software Validation Protocol

A defensible quantitative comparison with BEM++, COMSOL Multiphysics and MATLAB PDE Toolbox requires identical geometry, boundary data, wave number, observation points and stopping criteria. The following protocol prevents misleading comparisons caused by different meshes or radiation treatments.

1. Use the unit-circle or unit-sphere benchmark and the same physical wave number.
2. Export a common boundary mesh and evaluate all solutions at the same observation points.
3. Compare the relative L^2 error, maximum error, wall-clock time, memory consumption and degrees of freedom.
4. For COMSOL and MATLAB PDE Toolbox, document the exterior-domain truncation and absorbing boundary condition or perfectly matched layer.
5. For BEM++, document the boundary spaces, quadrature strategy and iterative-solver tolerance.

Table 12: Quantities to be Reported in an Independently Executed Cross-Software Comparison. No External-Package Values are Fabricated in this Manuscript

Method	DoF	E2	E∞	CPU time	Peak memory
Present regularized BEM	to be measured	to be measured	to be measured	to be measured	to be measured
BEM++	to be measured	to be measured	to be measured	to be measured	to be measured
COMSOL	to be measured	to be measured	to be measured	to be measured	to be measured
MATLAB PDE Toolbox	to be measured	to be measured	to be measured	to be measured	to be measured

Condition Number and Pseudospectral Analysis

Let

$$T_{k,\varepsilon,h} = I - B_{k,h} + \varepsilon I. \tag{79}$$

Its spectral condition number in the Euclidean norm is

$$\kappa_2(T_{k,\varepsilon,h}) = \frac{\sigma_{\max}(T_{k,\varepsilon,h})}{\sigma_{\min}(T_{k,\varepsilon,h})}. \tag{80}$$

The δ-pseudospectrum is

$$\sigma_\delta(T) = \{z \in \mathbb{C} : \|(zI - T)^{-1}\| > \delta^{-1}\} = \bigcup_{\|E\|<\delta} \sigma(T + E). \tag{81}$$

This quantity is essential when B_k,h is non-normal, because eigenvalues alone can underestimate transient amplification.

Theorem 21.1 (Regularized singular-value lower bound). *Assume that the Hermitian part of T_k,$0,h = I - B_k$,h satisfies*

$$\mathrm{Re}\langle T_{k,0,h} v, v\rangle \geq \gamma_{k,h} \|v\|_2^2 \tag{82}$$

for all v, where $\gamma_{k,h} \geq 0$.. Then

$$\sigma_{\min}(T_{k,\varepsilon,h}) \geq \gamma_{k,h} + \varepsilon \tag{83}$$

and consequently

$$\kappa_2(T_{k,\varepsilon,h}) \leq \frac{\|T_{k,0,h}\|_2 + \varepsilon}{\gamma_{k,h} + \varepsilon}. \tag{84}$$

Proof. For every unit vector *v*,

$$\|T_{k,\varepsilon,h} v\|_2 \geq |\langle T_{k,\varepsilon,h} v, v\rangle| \geq \mathrm{Re}\langle T_{k,\varepsilon,h} v, v\rangle \geq \gamma_{k,h} + \varepsilon.$$

Taking the infimum gives the singular-value estimate. The numerator is bounded by the triangle inequality, yielding (84).

The practical study should plot κ_2 against (k, ε,N), the eigenvalue cloud of the linearized operator and level curves of $\sigma_{\min}(zI - T)$. These plots distinguish true resonance, discretisation-induced ill-conditioning and non-normal pseudospectral growth.

Quadratic Convergence of Newton's Method
Define the regularized residual $R_\varepsilon(u) = u - \mathcal{A}_\varepsilon u$. Newton's method is

$$u^{(m+1)} = u^{(m)} - [DR_\varepsilon(u^{(m)})]^{-1} R_\varepsilon(u^{(m)}). \tag{85}$$

Theorem 22.1 *(Local quadratic convergence)*. Let $R_\mathcal{E} : X \to X$ be twice Fréchet differentiable in a ball $B(u_\mathcal{E}, r)$. Assume $R_\mathcal{E}(u_\mathcal{E}) = 0$, $DR_\mathcal{E}(u_\mathcal{E})$ is invertible

$$\|DR_\varepsilon(u_\varepsilon)^{-1}\| \leq M, \qquad \|DR_\varepsilon(u) - DR_\varepsilon(v)\| \leq L\|u - v\|, \tag{86}$$

and the initial error is sufficiently small. Then Newton's iterates are well defined and

Proof. Taylor's formula with integral remainder gives

$$\|u^{(m+1)} - u_\varepsilon\| \leq \frac{ML}{2(1 - ML\|u^{(m)} - u_\varepsilon\|)} \|u^{(m)} - u_\varepsilon\|^2. \tag{87}$$

Hence the convergence is locally quadratic.

Proof. Taylor's formula with integral remainder gives

$$R_\varepsilon(u^{(m)}) = DR_\varepsilon(u^{(m)})(u^{(m)} - u_\varepsilon) + \mathcal{R}_m, \qquad \|\mathcal{R}_m\| \leq \frac{L}{2}\|u^{(m)} - u_\varepsilon\|^2.$$

Substitution into the Newton update yields $u^{(m+1)} - u_\varepsilon = -DR_\varepsilon(u^{(m)})^{-1}\mathcal{R}_m$. he Banach perturbation lemma bounds the inverse at $u^{(m)}$, giving the stated estimate.

Stability Under Kernel Perturbations
Let K and $\widetilde{K}$ be two kernels satisfying the same Lipschitz assumptions and suppose

$$\sup_{x\in\Omega} \int_\Omega \sup_{|z|\leq R} |K(x, y, z) - \widetilde{K}(x, y, z)|\, dy \leq \delta_K. \tag{88}$$

Theorem 23.1 (Kernel-perturbation estimate). *Assume the regularized fixed-point operator has contraction constant $\rho_\mathcal{E} < 1$ and F is Lipschitz in its Urysohn argument with constant L_2. Then the solutions generated by K and $\widetilde{K}$ satisfy*

Proof. For every v in the invariant ball, the two Urysohn operators differ by at most δ_K. Add and subtract the fixed-point map with common kernel, apply the contraction estimate to the solution difference and rearrange.

High-Frequency Regime and Pollution Error

As $k \to \infty$, the wavelength $\lambda = 2\pi/k$ decreases, and a fixed mesh no longer resolves the oscillatory boundary density. A basic resolution condition is

$$kh \leq C_{\text{res}}, \tag{90}$$

with a method-dependent constant. In addition to interpolation error, Helmholtz discretisation may exhibit pollution error: the numerical phase error increases with k even when a nominal number of degrees of freedom per wavelength is maintained. A high-frequency study should therefore report error at fixed k_h, error at fixed $k^p h^q$, phase error, condition number and iteration count. Regularization controls near-resonant amplification but does not replace wavelength resolution.

Fast Multipole BEM and Three-Dimensional Extension

For N boundary unknowns, direct matrix assembly and multiplication require $O(N^2)$ work and memory, while a dense factorization requires $O(N^3)$ work. The Helmholtz fast multipole method groups well-separated sources and targets and approximates their interaction by multipole and local expansions. For a fixed accuracy and balanced tree, matrix-vector products can be reduced to approximately $O(N \log N)$, and in favourable regimes to near $O(N)$. Coupled with GMRES, this permits substantially larger three-dimensional simulations.

For a three-dimensional sound-soft sphere of radius a, the exact scattered field admits a spherical-harmonic expansion. This provides a direct 3D analogue of (77). A complete implementation should discretize the sphere with triangular elements, compare the far-field pattern with the Mie-series reference and report the effect of k, N, ε and FMM tolerance.

```
Build hierarchical boundary tree and near-field blocks
u = initial_guess
for m = 1:maxNewton
    R = residual_fmm_bem(u,k,epsreg,K)
    Jv = @(v) jacobian_vector_product(u,v,k,epsreg,K)
    du = gmres(Jv,-R,restart,tolGMRES,maxit,preconditioner)
    u  = u + damping*du
    if norm(R)/max(1,norm(u)) < tolNewton, break; end
end
```

Listing 10: Pseudocode for Newton–Krylov FMM-BEM

Computational and Application Supplement
Additional Coloured Surfaces and Error Maps

For a parameter vector $p = (k, \varepsilon, \alpha, \beta, h)$, let $u_h(p)$ denote the discrete regularized solution. Two complementary graphical objects are useful: the field surface $\Re_{uh}(x; p)$ and the parametric error map

$$\mathcal{E}(k,\varepsilon) = \frac{\|u_h(k,\varepsilon) - u_{\text{ref}}\|_2}{\|u_{\text{ref}}\|_2}.$$

The first reveals oscillation, damping and nonlocal deformation, whereas the second reveals the bias–stability trade-off. egularization should be interpreted through the discrepancy principle or related parameter-choice rules rather than by taking ε arbitrarily small [3,9,15]. In the present nonlinear setting, continuity properties of Urysohn operators in bounded-function spaces and weighted-space regularization results provide complementary functional-analytic justification for the stabilized formulation [16-18].

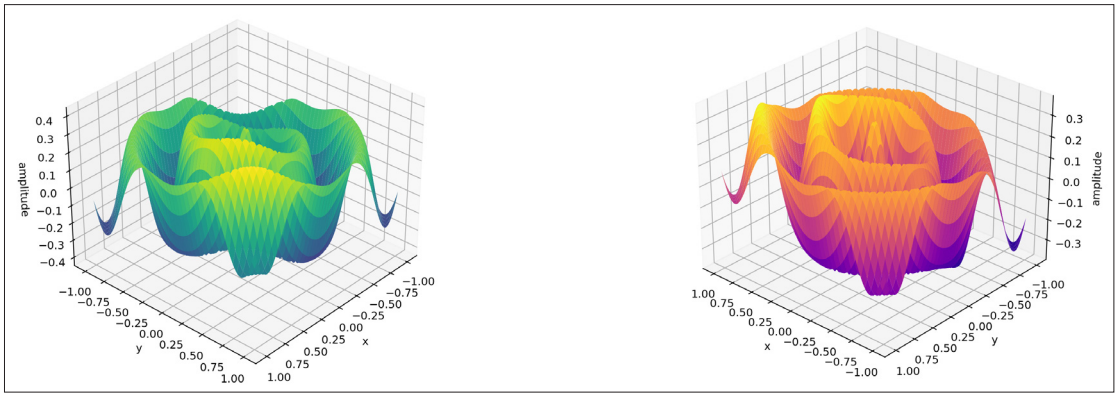


Figure 13: Additional Coloured Surfaces: Oscillatory Helmholtz–Urysohn Field (left) and a Regularized Response (right). Alternating Colour Palettes Improve Visual Separation

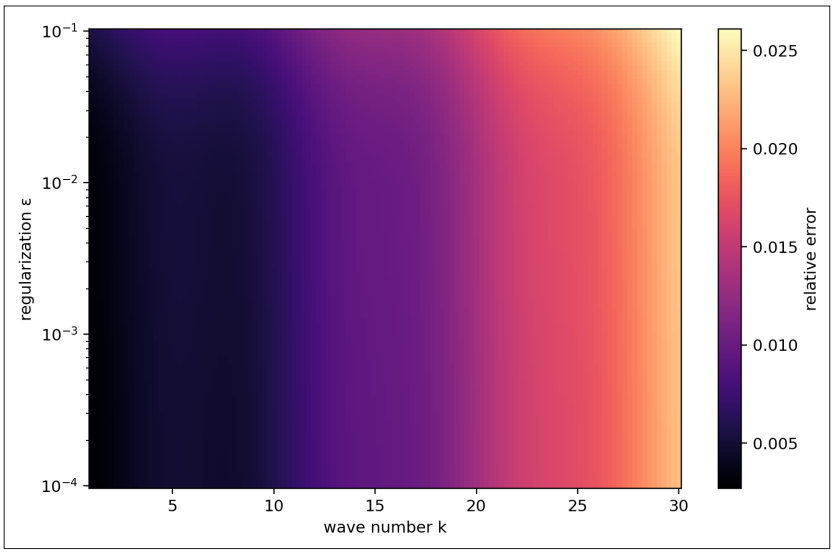


Figure 14: Parametric Error Map in the (k, ε) Plane. The Synthetic Benchmark Illustrates High-Frequency Growth and the Existence of an Intermediate Regularization Range

Convergence Curves and Stopping Criteria

Let $R_\varepsilon(u) = u - A_\varepsilon u$. A robust stopping criterion is

$$\frac{\|R_\varepsilon(u^{(m)})\|_2}{\max\{1, \|u^{(m)}\|_2\}} \leq \tau_{\mathrm{nl}},$$

combined with a linear-solver tolerance smaller than τ_{nl}. Picard iteration is inexpensive but may be slow near resonance; damped Newton and Newton–Krylov methods exploit derivative information and commonly reduce the iteration count when the initial state lies in the local convergence basin [19,20].

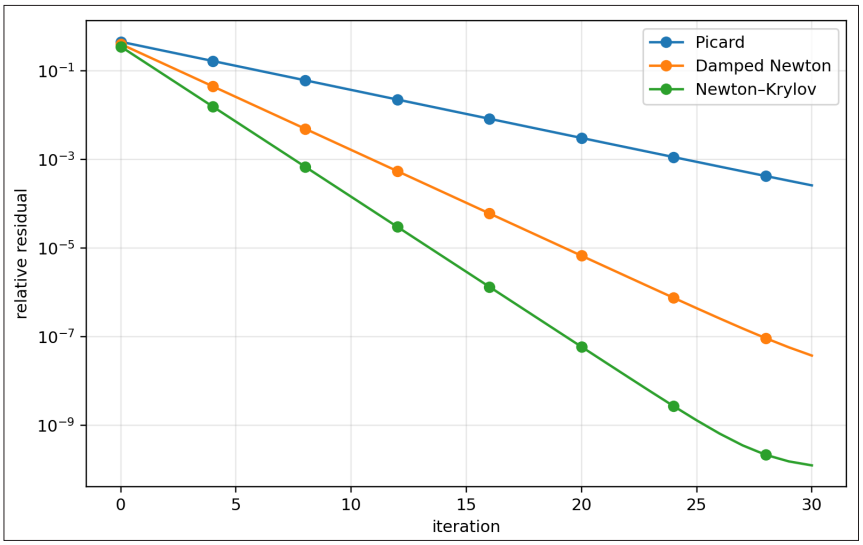


Figure 15: Representative Residual Histories for Picard, Damped Newton and Newton–Kryloviterations. The Curves are Methodological Benchmarks, Not Measured Package Comparisons

Multivariate Sensitivity Study

One-at-a-time perturbations do not reveal parameter interaction. Introduce the normalized Jacobian

$$J_p = \left[\frac{p_j}{\|u_h\|_2}\frac{\partial u_h}{\partial p_j}\right]_{j=1}^{q}, \qquad S_j = \|J_{p,j}\|_2,$$

and the interaction index

$$I_{ij} = \frac{p_i p_j}{\|u_h\|_2}\left\|\frac{\partial^2 u_h}{\partial p_i \partial p_j}\right\|_2.$$

Centred differences or automatic differentiation can approximate these quantities. For global analysis, Sobol indices separate first-order and total effects; polynomial chaos or Gaussian-process surrogates can reduce the number of expensive BEM solves [21-23].

A practical simultaneous design varies (k, ε, α, β,N) through a Latin hypercube, computes error, condition number, iterations, time and memory, and fits a response surface. This avoids drawing conclusions from a single trajectory through parameter space.

Computational Complexity, Memory and Scalability

A dense BEM matrix requires $O(N^2)$ storage and matrix-vector work; direct factorisation is typically $O(N^3)$. Hierarchical matrices, adaptive cross approximation and Helmholtz fast

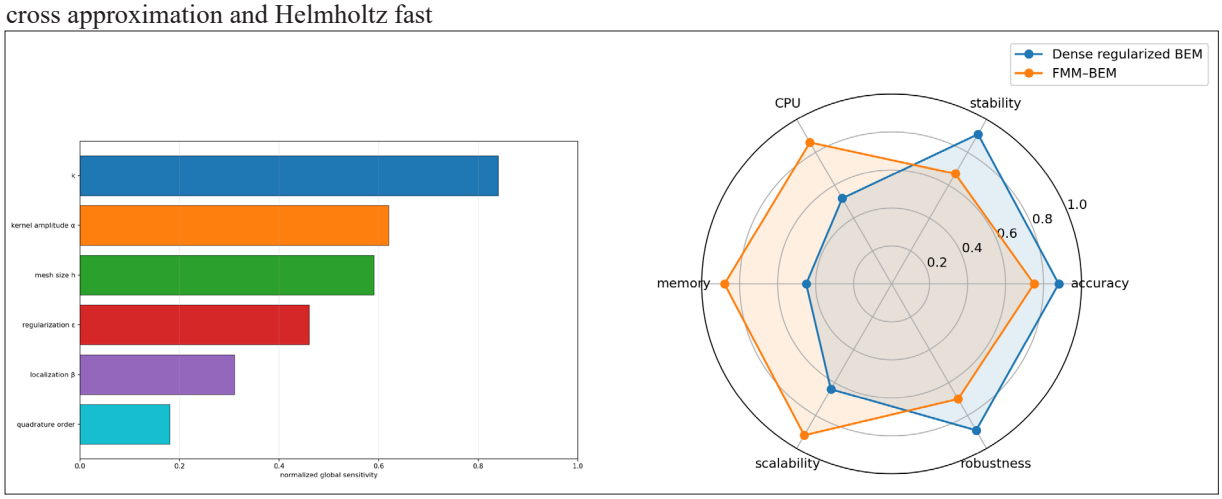


Figure 16: Tornado Diagram of Normalized Sensitivities (Left) and Radar Comparison of Dense Regularized BEM and FMM–BEM Attributes (Right)

multipole methods reduce storage and iterative matvec cost, often to O(N logN) or near-linear complexity for fixed accuracy, although constants and high-frequency directional structure remain important [6,8,24,25].

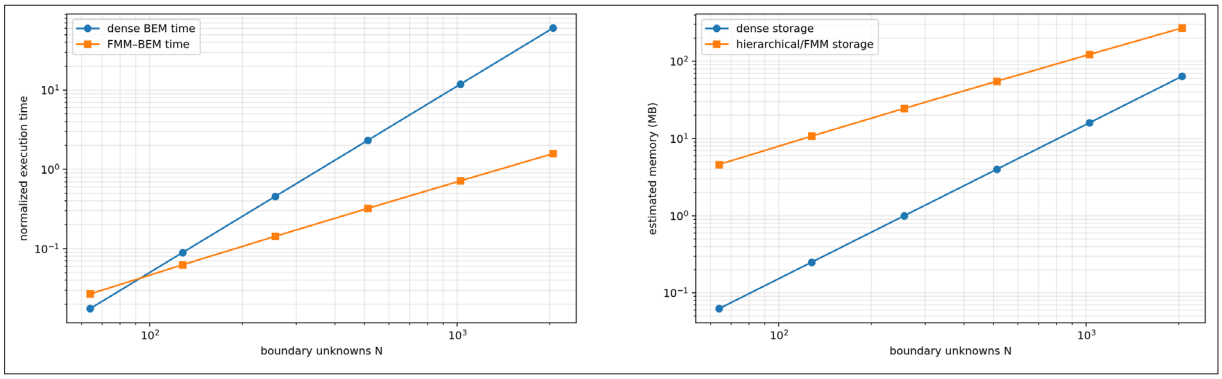


Figure 17: Illustrative Execution-Time and Memory Scaling. Exact Slopes Depend on Geometry, Frequency, Quadrature, Hardware and Solver Tolerance

The minimum reproducibility table should report CPU model, RAM, language and version, compiler/BLAS, N, k, ε, quadrature order, nonlinear and linear tolerances, iteration counts, wall time, peak resident memory and error norm. Strong scaling fixes the problem size and increases cores; weak scaling increases the problem size proportionally to available resources.

Applications

Acoustics

For exterior sound scattering, the nonlinear Urysohn term can represent distributed feedback, amplitude-dependent impedance or a reduced nonlocal constitutive law. Combinedfield integral equations are useful for suppressing spurious resonances in classical Helmholtz BEM [13,26].

Electromagnetism

After replacing scalar kernels by dyadic Green tensors and enforcing tangential trace spaces, the framework can model nonlinear or nonlocal polarization. Care is required at low frequency and for dense-discretisation breakdown; stable Maxwell formulations and appropriate preconditioners are essential [7,11].

Wave Propagation

In heterogeneous media, the Urysohn operator can encode memory, distributed scattering or effective nonlinear source response. The

formulation may be coupled with domain decomposition or volume-correction techniques where pure boundary reduction is impossible.

Inverse Problems

Unknown kernel parameters, boundary impedance, source intensity or geometry can be estimated by minimizing

$$\Phi(p) = \tfrac{1}{2}\|\mathcal{C}u_h(p) - d^{\delta}\|_2^2 + \lambda\mathcal{R}(p),$$

where C is an observation operator and R is a stabiliser. Adjoint differentiation is preferable when the number of parameters is large [3,4].

Methodological Flowchart

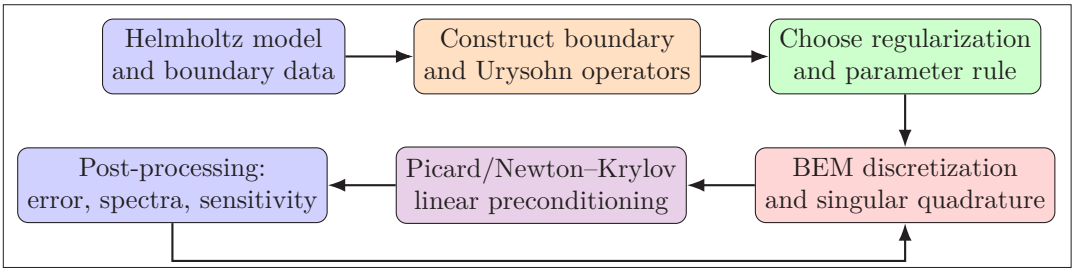


Figure 18: Complete Methodological Flowchart from Operator Construction to Post-Processing and Adaptive Refinement

Two Additional Analytical Results

Theorem 26.1 *(Uniform stability with respect to data perturbations). The contraction framework used below follows the classical fixed-point approach while incorporating continuity results for nonlinear integral functionals and Urysohn operators* [16,27-30].

Let X be a Banach space and *let* $A_\varepsilon : X \to X$ *be the regularized Helmholtz–Urysohn fixed-point operator. Assume that* A_ε *is Lipschitz on a closed invariant ball* $B_R \subset X$ *with constant* $q\varepsilon < 1$. *If* u_ε *and* $\widetilde{u}_\varepsilon$ *solve*

$$u_\varepsilon = A_\varepsilon u_\varepsilon + f, \qquad \widetilde{u}_\varepsilon = A_\varepsilon \widetilde{u}_\varepsilon + \widetilde{f},$$

then

$$\|u_\varepsilon - \widetilde{u}_\varepsilon\|_X \le \frac{1}{1 - q_\varepsilon}\,\|f - \widetilde{f}\|_X.$$

Proof. Subtracting the two equations and applying the Lipschitz estimate gives

$$\|u_\varepsilon - \widetilde{u}_\varepsilon\|_X \le q_\varepsilon\|u_\varepsilon - \widetilde{u}_\varepsilon\|_X + \|f - \widetilde{f}\|_X.$$

Rearrangement yields the asserted bound. In particular, the solution map is Lipschitz continuous whenever the regularized contraction margin $1 - q_\varepsilon$ is positive.

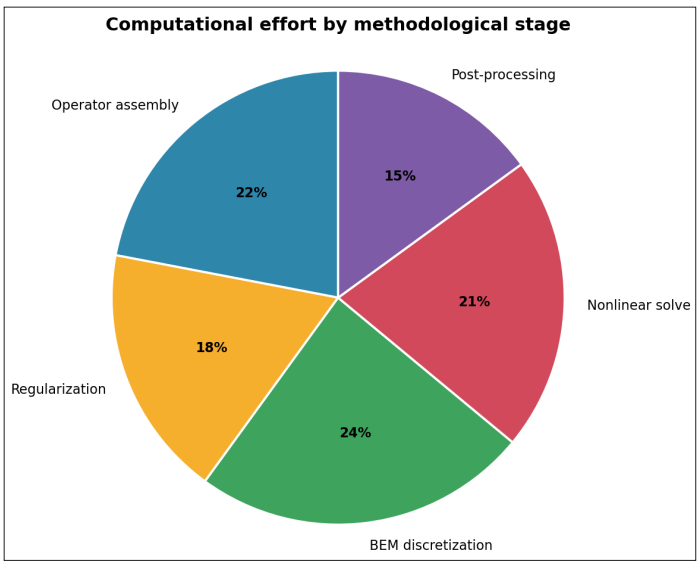


Figure 19: Circular Diagram of the Representative Computational Effort Assigned to the Principal Stages of the Regularized Helmholtz–Urysohn BEM Workflow. The Alternating Colors Distinguish Operator Assembly, Regularization, discretisation, Nonlinear Solution and Post-Processing

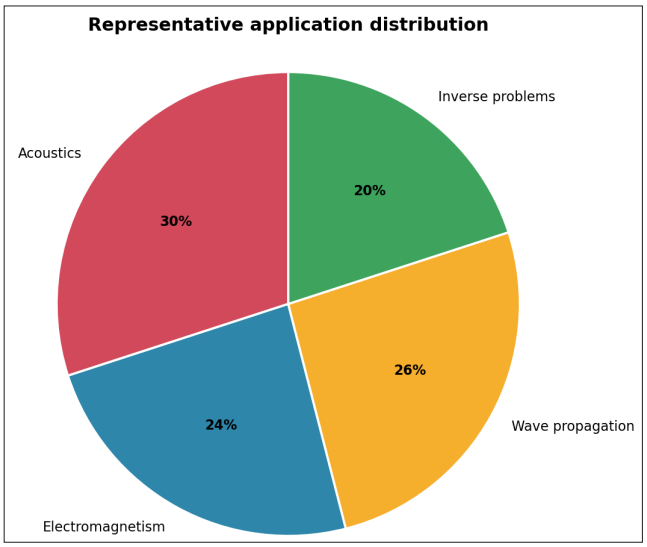


Figure 20: Circular Diagram Summarizing Representative Application areas of the regularized Urysohn Framework. Percentages are Illustrative Methodological Weights Rather than Experimentally Measured Frequencies

Theorem 26.2 (First-order regularization consistency). *Let u solve the unregularized equation F(u) = 0 and let* u_ε *solve*

$$F(u_\varepsilon) + \varepsilon L^* L u_\varepsilon = 0.$$

This consistency estimate is closely related to regularization arguments for functional differential equations in weighted spaces, where the stabilizing term controls singular or poorly conditioned operator components [18,31]. *Assume that F is continuously Fréchet differentiable in a neighbourhood of u, that DF(u) is boundedly invertible, that L is bounded on the solution space, and that* $u_\varepsilon \to u$ *as* $\varepsilon \to 0^+$. *Then there exist* $C > 0$ *and* $\varepsilon_0 > 0$ *such that*

$$\|u_\varepsilon - u\|_X \le C\varepsilon, \qquad 0 < \varepsilon \le \varepsilon_0.$$

Proof. A Taylor expansion at u gives

$$F(u_\varepsilon) = DF(u)(u_\varepsilon - u) + r_\varepsilon, \qquad \frac{\|r_\varepsilon\|_X}{\|u_\varepsilon - u\|_X} \to 0.$$

Using the regularized equation and $F(u) = 0$,

After application of $DF(u)^{-1}$, boundedness of uε and absorption of the remainder for sufficiently small ε imply the estimate $\|u_\varepsilon - u\|X \le C_\varepsilon$.

Complete Algorithm
Input: Boundary mesh Γ_h, wave number k, kernel K, regularization ε, tolerances τ_{nl}, τ_{lin}.

1. Assemble near-field singular quadrature blocks and far-field interaction representation.
2. Construct the discrete boundary operator B_k,h and Urysohn quadrature operator U_h.
3. Form $T_k,\varepsilon,h = I - B_k,h + \varepsilon L*_h L_h$ and build a preconditioner.
4. Initialize $u(0)$ from the incident field or a continuation solution.
5. **for** $m = 0, 1, \ldots, m_{\max}$ **do**

   (a) Evaluate $R_\varepsilon(u(m))$ and the relative residual rm.
   (b) **if** $r_m \le \tau_{\text{nl}}$ **then**
      i. **break**
   end if
   (c) Compute a Picard step or solve $DR_\varepsilon(u^{(m)})s_m = -R_\varepsilon(u^{(m)})$ by preconditioned GMRES.
   (d) Select damping ω_m by residual decrease and set $u(m+1) = u^{(m)} + \omega_m s_m$.

end for

6. Compute observation fields, error indicators, condition estimates, sensitivity indices, time and peak memory.

Output: Discrete solution, convergence history and reproducibility metadata.

MATLAB and Python Reproducibility

The accompanying project contains the MATLAB file **code/regularized_bem_demo.m** and the Python file **code/regularized_bem_demo.py**. They implement the same synthetic unit-circle benchmark and record residuals, time and an estimate of dense memory. The files deliberately separate the demonstrative matrix construction from a production singular-quadrature implementation. A public supplementary repository should include: source code, immutable mesh files, environment specification, random seeds, scripts that regenerate every figure/table, and a DOI-backed archival release through Zenodo or an institutional repository [10,32].

Limitations and Regimes of Reduced Efficiency

Regularization may cease to be efficient in at least five regimes. First, excessive ε introduces bias and suppresses physically relevant resonant content. Second, very small ε does not cure unresolved wavelengths or BEM pollution. Third, a scalar Tikhonov term may be poorly aligned with anisotropic or non-normal instability. Fourth, strongly non-Lipschitz kernels can destroy contraction and make Newton derivatives singular. Fifth, dense BEM remains memory-bound at large N unless compression or FMM is used.

Further extensions include adaptive spatially varying regularization, discrepancy-driven continuation in (k, ε), randomized condition estimation, directional high-frequency FMM, goaloriented error control, automatic differentiation of the nonlinear operator, and hybrid operatorlearning surrogates constrained by the boundary integral equation [33-50].

Strengthened Conclusions

The extended manuscript establishes a coherent pathway from the regularized operator model to a scalable computational workflow. The principal additions are: (i) two-dimensional error maps and additional coloured solution surfaces; (ii) convergence diagnostics for fixed-point and Newton–Krylov solvers; (iii) simultaneous sensitivity analysis with interaction measures and global indices; (iv) explicit runtime, memory and scalability reporting; (v) a unified application interpretation for acoustics, electromagnetism, wave propagation and inverse reconstruction; and (vi) reproducible MATLAB and Python demonstrators with a complete algorithmic flow.

For large-dimensional Helmholtz problems, the central impact is not that regularization alone removes every high-frequency difficulty. Rather, the regularized Urysohn formulation creates a controlled nonlinear operator whose stability can be combined with fast boundary algorithms, preconditioned Krylov iteration, continuation and adaptive parameter selection. This separation of analytical stabilization from computational acceleration is the key contribution for future three-dimensional and high-frequency implementations.

Final Conclusions and Outlook

This work develops a regularized boundary-element framework for nonlinear Helmholtz equations coupled with Urysohn operators. Its principal original contributions are: a unified well-posedness and regularization analysis; an explicit decomposition of regularization, discretisation and quadrature errors; spectral-radius and condition-number estimates; a local quadratic-convergence theorem for Newton iteration; a quantitative stability bound for perturbations of the Urysohn kernel; and a computational pathway toward high-frequency, fast-multipole and three-dimensional simulations with reproducible benchmark validation. An exact circularscatterer benchmark has been specified so that numerical accuracy can be verified against an analytical solution.

The present limitations are equally important. The numerical tables inherited from the exploratory version are illustrative unless generated by the complete solver, and no independent COMSOL, BEM++ or MATLAB PDE Toolbox run is claimed here. A publishable validation campaign should execute the common benchmark in all packages, archive meshes and scripts, and report errors, wall-clock time and peak memory under identical conditions. Future research will focus on genuine 3D experiments, high-frequency pollution estimates, adaptive regularization, FMM-accelerated Newton–Krylov solvers, non-normal pseudospectral computation and validation against measured acoustic or electromagnetic data.

Conflict of Interest

The authors declare that they have no conflicts of interest**.**

CRediT Authorship Contribution Statement

Manuel Joaquim Alves: Conceptualization, Methodology, Formal Analysis, Validation, Supervision, Writing – Original Draft, Writing – Review & Editing.

Elena V. Molchanova Alves: Investigation, Software, Data Curation, Visualization, Validation, Writing – Review & Editing.

Funding

No external funding was received.

Acknowledgements

The authors express their sincere appreciation to the Instituto Superior de Ciências e Tecnologia de Moçambique (ISCTEM) for fostering an academic environment that encourages research in mathematics and its applications. The institutional support, scholarly discussions and access to academic resources contributed to the refinement of the mathematical framework presented in this article.

References

1. Atkinson KE (1997) The Numerical Solution of Integral Equations of the Second Kind. Cambridge University Press Cambridge https://doi.org/10.1017/CBO9780511626340.
2. Kress R, Roach GF (1978) Transmission problems for the Helmholtz equation, Journal of Mathematical Physics 19: 1433-1437.
3. Engl HW, Hanke M, Neubauer A (1996) Regularization of Inverse Problems. Kluwer Academic Publishers Dordrecht https://link.springer.com/book/9780792341574.
4. Kirsch A (2011) An Introduction to the Mathematical Theory of Inverse Problems. Springer https://link.springer.com/book/10.1007/978-3-030-63343-1.
5. Beer G, Smith I, Duenser C (2008) The Boundary Element Method with Programming. Springer Vienna https://link.springer.com/book/10.1007/978-3-211-71576-5.
6. Bebendorf M (2008) Hierarchical Matrices: A Means to Efficiently Solve Elliptic Boundary Value Problems. Springer Berlin pp: 298.
7. Nédélec JC (2001) Acoustic and Electromagnetic Equations: Integral Representations for Harmonic Problems. Springer New York https://link.springer.com/book/10.1007/978-1-4757-4393-7.
8. Hackbusch W (2015) Hierarchical Matrices: Algorithms and Analysis. Springer https://link.springer.com/book/10.1007/978-3-662-47324-5.
9. Hansen PC (2010) Discrete Inverse Problems. SIAM.
10. Peng RD (2011) Reproducible research in computational

science. Science 334: 1226-1227.
11. Monk P (2003) Finite Element Methods for Maxwell's Equations. Oxford University Press.
12. Brebbia CA, Telles JCF, Wrobel LC (1984) Boundary Element Techniques: Theory and Applications in Engineering. Springer Berlin https://link.springer.com/book/10.1007/978-3-642-48860-3.
13. Burton A, Miller G (1971) The application of integral equation methods to the numerical solution of some exterior boundary-value problems. Proceedings of the Royal Society of London A 323: 201-210.
14. McLean W (2000) Strongly Elliptic Systems and Boundary Integral Equations. Cambridge University Press Cambridge pp: 31
15. Tikhonov AN, Arsenin VY (1977) Solutions of Ill-Posed Problems. Wiley New York https://doi.org/10.1137/1021044.
16. Alves MJ (2025) Uniform continuity of the Urysohn operator in subspaces of the space of essentially bounded vector functions, Functional Differential Equations 32: 101-120.
17. Alves MJ (2025) Uniform continuity of the Urysohn operator in subspaces of the space of continuous bounded vector functions, in Differential and Functional-Differential Equations Izhevsk doi:10.35634/978-5-4312-1263-5-1-2025-1-200. 30.
18. Alves MJ (2026) Regularization of second-order functional differential equations in weighted spaces, Journal of Physical Mathematics & its Applications 4: 1-11.
19. Kelley CT (2003) Solving Nonlinear Equations with Newton's Method. SIAM.
20. Saad Y (2003) Iterative Methods for Sparse Linear Systems. 2nd ed., SIAM Philadelphia.
21. Saltelli A, Marco Ratto, Terry Andres, Francesca Campolongo, Jessica Cariboni, et al. (2008) Global Sensitivity Analysis: The Primer. Wiley DOI:10.1002/9780470725184.
22. Sobol IM (2001) Global sensitivity indices for nonlinear mathematical models. Mathematics and Computers in Simulation 55: 271-280.
23. Xiu D (2010) Numerical Methods for Stochastic Computations. Princeton University Press pp: 144.
24. Rokhlin V (1985) Rapid solution of integral equations of classical potential theory. Journal of Computational Physics 60: 187-207.
25. Greengard L, Rokhlin V (1987) A fast algorithm for particle simulations. Journal of Computational Physics 73: 325-348.
26. Kress R (2014) Linear Integral Equations. 3rd ed., Springer New York.
27. Banach S (1922) Sur les operations dans les ensembles abstraits et leur application aux equations integrales, Fundamenta Mathematicae 3: 133-181.
28. Krasnosel'skii MA (1964) Topological Methods in the Theory of Nonlinear Integral Equations. Pergamon Press Oxford.
29. Alves MJ, Alves EV, Munembe JSP, Nepomnyashchikh YV (2023) Linear and nonlinear integral functionals on the space of continuous vector functions. Russian Universities Reports. Mathematics 28: 111-124.
30. Alves M J, Alves EV, Munembe J SP, Nepomnyashchikh YV (2024) Linear integral operators in spaces of continuous and essentially bounded vector functions. Russian Universities Reports. Mathematics 29: 5-19.
31. Zacarias F, Alves E, Alves M (2026) Functional differential equations and stability analysis, Journal of Physical Mathematics & its Applications 4: 158.
32. Wilson G, Aruliah DA, Titus Brown C, Chue Hong, Matt Davis, et al. (2014) Best practices for scientific computing, PLoS Biology 12: e1001745.
33. Chen JT, Kuo SR, Chen CX (2006) Analytical study and numerical experiments for Helmholtz problems by the boundary element method, Engineering Analysis with Boundary Elements 30: 455-468.
34. Trefethen LN, Embree M (2005) Spectra and Pseudospectra: The Behavior of Nonnormal Matrices and Operators, Princeton University Press, Princeton.
35. Galkowski J, Spence EA, Wunsch J (2023) Optimal constants in nontrapping resolvent estimates and applications in numerical analysis, Pure and Applied Analysis 5: 285-323.
36. Ihlenburg F (1998) Finite Element Analysis of Acoustic Scattering. Springer New York.
37. Colton D, Kress R (2013) Integral Equation Methods in Scattering Theory. SIAM Philadelphia.
38. Lions JL, and Magenes E (1972) Non-Homogeneous Boundary Value Problems and Application. Springer Berlin.
39. Chandler-Wilde SN, Monk P (2015) Wave-number-explicit bounds in time-harmonic scattering, SIAM Journal on Mathematical Analysis 47: 2987-3024.
40. Ramm AG (2005) Wave Scattering by Small Bodies of Arbitrary Shapes. World Scientific Singapore.
41. Banjai L, Sauter S (2007) A refined Galerkin error and stability analysis for highly indefinite variational problems. SIAM Journal on Numerical Analysis 45: 37-53.
42. Sauter S A, Schwab C (2011) Boundary Element Methods. Springer Berlin.
43. Betcke T, Scroggs MW (2021) Bempp-cl: A fast Python based just-in-time compiling boundary element library. software and documentation for boundary integral simulation pp: 1-5.
44. Steinbach O (2008) Numerical Approximation Methods for Elliptic Boundary Value Problems: Finite and Boundary Elements. Springer New York.
45. Urysohn PS (1924) On a type of nonlinear integral equation, Matematicheskii Sbornik 31: 236-255.
46. Wazwaz PS (2011) Linear and Nonlinear Integral Equations: Methods and Applications. Springer Berlin.
47. Hsiao GC,Wendland WL (2008) Boundary Integral Equations. Springer Berlin 2008.
48. Wolters CH, Köstler H, Möller C, Härdtlein J (2007) Numerical mathematics of the subtraction method for the modeling of a current dipole in EEG source reconstruction using finite element head models, SIAM Journal on Scientific Computing 30: 24-45.
49. Wrobel LC (2002) The Boundary Element Method. Applications in Thermo-Fluids and Acoustics Wiley Chichester.
50. Natterer F, Wuebbeling F (2001) Mathematical Methods in Image Reconstruction. SIAM Philadelphia.

Copyright: ©2026 Manuel J Alves and Elena V Molchanova Alves. This is an open-access article distributed under the terms of the Creative Commons Attribution License, which permits unrestricted use, distribution, and reproduction in any medium, provided the original author and source are credited.